

Figures of Merit for Durable Icephobic Coatings

by

Sina Nazifi Takan Tappeh

A thesis submitted to the Mechanical Engineering Department

in partial fulfillment of the requirements for the degree of

MASTER OF SCIENCE

in Mechanical Engineering

Chair of Committee: Dr. Hadi Ghasemi

Committee Member: Dr. Haleh Ardebili

Committee Member: Dr. Karim Alamgir

University of Houston

December 2021

Copyright 2021, Sina Nazifi Takan Tappeh

## **ACKNOWLEDGMENTS**

I would like to thank my esteemed supervisor – Dr. H. Ghasemi for his invaluable supervision, support and tutelage during the course of my PhD degree. My gratitude extends to the National Science Foundation for the funding opportunity to undertake my studies at the Department of Mechanical Engineering, University of Houston. Additionally, I would like to express gratitude to Dr. P. Irajizad for his treasured support and comments which was really influential in shaping my experiment methods and critiquing my results. My appreciation also goes out to my family and friends for their encouragement and support all through my studies.

## **ABSTRACT**

From aviation systems and infrastructures to energy systems, icephobic surfaces play a critical role in humanity's daily lives. However, developing these surfaces for low-temperature applications remains a challenge. In the last few decades, a few forms of icephobic surfaces are developed including liquid-infused, non-wetting, and hydrated surfaces. However, their practical applications are limited due to high freezing temperatures, high ice adhesion, ice accretion, low mechanical durability, and high fabrication costs. Here, we present a comprehensive definition for icephobicity through thermodynamics, heat transfer, and mechanics of the ice/water interfaces. To accurately predict ice growth rates on different substrates and under different wind conditions, mathematical models are developed based on the conservation laws. We elucidate the mechanisms that nanoscale physics could be used to develop exceptional icephobic surfaces. A method for ice adhesion measurement is presented that uses physics of fracture at ice-icephobic material interfaces to eliminate discrepancies between reported ice adhesions from different laboratories. In addition, a comprehensive set of durability metrics is casted that includes mechanical, environmental, and chemical durability aspects. Through above knowledge, a thorough framework for comparing the performance of state-of-the-art icephobic surfaces is developed and the main weaknesses are identified.

# TABLE OF CONTENTS

<b>ACKNOWLEDGMENTS.....</b>	<b>iii</b>
<b>ABSTRACT .....</b>	<b>iv</b>
<b>TABLE OF CONTENTS .....</b>	<b>v</b>
<b>LIST OF TABLES.....</b>	<b>vii</b>
<b>LIST OF FIGURES.....</b>	<b>viii</b>
<b>I. INTRODUCTION.....</b>	<b>1</b>
<b>II. ICEPHOBIC SURFACES .....</b>	<b>5</b>
Superhydrophobic Surfaces (SHS) .....	10
Liquid Infused Porous Surfaces (SLIPS) .....	11
Liquid Infused Surfaces (LIS).....	12
Interfacial Slippage .....	13
Stress-Localized Surfaces (SLS).....	13
Low Interfacial Toughness Surfaces (LITs) .....	14
Comparison .....	14
<b>III. MERITS FOR INDUSTRIES APPLICATION .....</b>	<b>17</b>
Ice Adhesion Performance .....	20
Mechanical Durability .....	20
Chemical Resistance .....	25

<b>IV. METROLOGY FOR ICE ADHESION .....</b>	<b>26</b>
Ice Nucleation .....	27
Ice Growth.....	35
Case I: Droplet in an environment without airflow .....	36
Case II: Droplet in an environment with external airflow .....	41
Freezing Delay .....	44
Ice Adhesion Strength.....	45
Methods for measurement.....	46
Centrifugal method.....	46
Peak force method.....	50
Tensile force method.....	56
Standard Procedure for measurement .....	57
<b>V. CONCLUSION .....</b>	<b>61</b>
<b>REFERENCES .....</b>	<b>62</b>

## LIST OF TABLES

Table 1 Ice adhesion measured by centrifugal force method.....	50
Table 2 Ice adhesion measured by peak force method .....	53
Table 3 Ice adhesion measured by peak shear force method .....	56
Table 4 Parameters for standard ice adhesion measurements .....	59

## LIST OF FIGURES

Figure 1 Icing problem in various applications .....	3
Figure 2 State-of-the-art icephobic surfaces .....	9
Figure 3 Ice adhesion on state of the art surfaces .....	15
Figure 4 Mechanical durability tests on state-of-the-art icephobic surfaces.....	21
Figure 5 Erosion tests result on state-of the-art coatings .....	24
Figure 6. Ice nucleolus on a subzero substrate.....	28
Figure 7 The surface factor for convex surfaces .....	30
Figure 8 The surface factor plotted for concave surfaces .....	31
Figure 9 Role of surface factor on ice nucleation on state-of-the-art material .....	33
Figure 10 Ice growth on a sub-zero substrate in absence of airflow .....	38
Figure 11 The predicted ice growth rates on a substrate.....	40
Figure 12 Ice growth on a sub-zero substrate under airflow condition .....	41
Figure 13 Schematic of centrifugal force method.....	47
Figure 14 Experimental setup for centrifugal ice adhesion measurement .....	48
Figure 15 Rotational shear test method.....	54
Figure 16 Schematic of shear stress method for ice adhesion measurement .....	55
Figure 17 Schematic of tensile force method.....	57
Figure 18 . Experimental setup used for ice adhesion measurement with the tensile method a) before and b) after detachment .....	57
Figure 19 Schematic of standard setup for ice adhesion measurement .....	60

## I. INTRODUCTION

Icing is a common occurrence in subzero climates where moisture is present [1–3], and it affects a wide range of industries from transportation systems [4–6], power transmission lines [7], and infrastructures [8,9] to energy systems [10-14]. Figure 1 shows Ice on aircraft can cause increased drag, loss of lift force, and catastrophic events. Ice on transmission systems can result in poles and towers collapsing and conductors rupturing. As a result of icing in cooling systems, their heat transfer rate is significantly reduced, resulting in inefficient operation. Ice storms are responsible for 10% of all power outages in the United States, according to Lawrence Berkeley Laboratory [15,16]. Financial markets for icephobic surfaces are around \$20 billion (B) annually [17], including \$10.17 billion (B) for aerospace, \$3 billion (B) for automobiles, \$2.3 billion (B) for infrastructures, and \$3 to \$5 billion (B) for power transmission lines. The coastguard and shipping industries are also significant markets for icephobic surfaces. In cold climates, this problem plays a critical role in daily human life rather than just economically. During the winter in the United States, about 3 million people experience power outages as a result of ice storms. Development of durable and high-performance icephobic surfaces remains challenging despite their vital role in economy and society. The main advantages of icephobic surfaces include low freezing temperatures, low ice accretion rates, low ice adhesion, and long-term durability. Figures of merit required for icephobic surfaces vary according to the application. For aircraft, low freezing temperature, low ice adhesion, and durability are the most critical characteristics. It

remains a challenge, despite significant progress, to develop surfaces that address all the necessary figures of merit (e.g. superhydrophobic surfaces [18-60], liquid-infused surfaces [20,61] and hydrated surfaces [62]).

To reduce ice accretion on the surfaces, it is essential to understand how ice forms on a surface, i.e. heterogeneous formation. On a surface, ice formation involves two stages: ice nucleation and subsequent ice growth. Ice nucleolus form on a sub-zero surface after a droplet of water is placed on it with a time delay. The Nucleation of ice is governed by the thermodynamics of the ice-water system and is described by the Gibbs energy barrier,  $\Delta G^*$ , which is strongly influenced by the surface factor,  $f(m, x)$ . In order to control ice nucleation, one can manipulate surface factor, which is a function of surface geometry, i.e. nano or micro, and free energy at the surface. The growth of ice occurs in a controlled manner by heat transfer following ice nucleation. Two extreme scenarios can be described for ice growth.



Figure 1 Icing problem in various applications

In the first case, ice is formed due to heat transfer from the substrate when there is no airflow around the substrate. In the second scenario, ice growth occurs in an environment with external airflow, and the rate of ice growth is largely determined by convective heat transfer. Any of the above theories about ice formation on a surface can be applied to an isolated, single droplet. However, in reality, the presence of many droplets on a surface can interfere with ice nucleation and growth, leading to ice bridges. Ice bridges arise because of vapor source-sink behavior due to the vapor pressure gradient between the frozen and adjacent liquid droplets.

The durability of an icephobic coating can be defined as its resistance to external agents that may interfere with its performance. Several factors can impair the durability of a coating, including environmental, chemical, and mechanical factors. UV-induced oxidation and thermal degradation are environmental elements that weaken the

durability of a coating. Corrosion and hydrolysis are two chemical agents which compromise the durability of coatings. In addition, mechanical failures in coatings include erosion, cracking, abrasion, and detachment from the substrate. All of the mentioned failures are affected by a variety of factors. As a result, the coating loses its icephobic properties. The durability of an icephobic coating is determined by how well it retains its icephobic properties over time.

## II. ICEPHOBIC SURFACES

In the following, we present state-of-the-art icephobic surfaces and analyze their characteristics using the metrics discussed above. Figure 8 shows a schematic representation of these surfaces. Figure 8a illustrates how superhydrophobic surfaces (SHS) are developed by micro/nano structuring hydrophobic surfaces (or hydrophilic surfaces). Surfaces of this type trap air and prevent wetting (Cassie-Baxter state) in order to minimize the effective contact area between stationary or dynamic subcooled droplets and the cold solid substrate [18-60]. The hydrophobic nature of these surfaces affects both the thermodynamics of ice nucleation (35,81,81,85,86,94,102,122-125) and mechanics of ice adhesion at the solid-ice interfaces (58,76). It has been demonstrated that TN is a function of the interfacial energy of solid-water mixtures and the dimension of micro/nano features through Gibbs energy barrier [78,126]. In the case of a given solid, the Gibbs energy barrier is not affected unless micro/nano features are of the same dimensional order as an ice embryo (a few nanometers) [78]. The fabrication of surfaces with such small features is challenging and expensive. Therefore, the median temperature for ice nucleation is in the range of -20 to -25 °C for most studied superhydrophobic surfaces [77]. On the other hand, the homogeneous ice nucleation temperature of bulk water is \*40 °C [127,128]. This temperature represents the lower limit for designing surfaces that are icephobic where nucleation occurs heterogeneously. As is discussed in Eq 4,  $\tau_{av}$  is also a function of Gibbs energy barrier. Accordingly, at a given temperature, the ice nucleation delay time is not affected unless the heterogeneous energy barrier is tuned. It should be noted that, although the droplet

contact area on superhydrophobic surfaces may be reduced, the molecular nature of the solid-ice interaction ( $W_a$ ) and the mechanical properties of the icephobic surface affect the ice adhesion strength. Various researchers have reported ice adhesion on superhydrophobic surfaces between 100 and 500 kPa, which is comparable to adhesion strengths measured on smooth metal surfaces ( $\sim 100$  kPa)[22,59,129–136]. As soon as frost forms between micro/nano structures on SHS, the water droplet sitting on the surface transforms into the Wenzel state and fills the micro/nano features. The adhesion of the ice can be even higher than on a smooth surface in this situation. Although extensive studies have been conducted on the icephobicity of SHS, low ice adhesion as well as mechanical durability of SHS have not yet been achieved.

A surface's icephobicity is sometimes measured based on a single or combination of material characteristics, such as water repellency or contact angle hysteresis. Despite the fact that these characteristics may indirectly affect the icephobicity of a surface, they are not directly associated with this characteristic. Numerous studies have demonstrated a correlation between water repellency and icephobicity. Dalton and his colleagues [72] developed a variety of surfaces that range from superhydrophilic to superhydrophobic. According to their findings, ice adhesion decreases as the contact angle of water on surfaces increases. On the most superhydrophobic surface, ice adhesion was reduced 18-fold in comparison to untreated aluminum. As reported by Kulinaich et al. [48], the correlation between ice adhesion and contact angle holds only when the hysteresis of the contact angle is low. The correlation between icephobicity and contact angle hysteresis was proposed.

Specifically, higher contact angle hysteresis indicated a larger surface area between the ice and the solid, resulting in greater ice adhesion. Accordingly, Cao et al. [73] developed a range of nanoparticle-polymer composites to examine the correlation between icephobicity and superhydrophobicity. The researchers found that icephobicity depends both on hydrophobicity and particle size (i.e. surface morphology). Meuler et al. [22] investigated the adhesion of ice to a wide variety of smooth steel discs coated with many hydrophobic coatings. Their work suggested that ice adhesion is correlated to the amount of adhesion work involved (i.e.  $W_a = L_V(1 + \cos r)$ ), and further reduction in adhesion can only be achieved by structuring surfaces. According to Meuler et al., [21], superhydrophobic surfaces can repel water droplets before freezing and thus become icephobic. On carbon-nanotube-based superhydrophobic surfaces, Zheng et al. [74] also found that water drop repellency before freezing plays a role in ice repellency. In a study by Jung et al. [75], the contact angle of superhydrophobic surfaces was found to increase the delay time for ice formation. The smoother the surface of a hydrophilic surface, the longer the delay time in ice formation. In designing icephobic surfaces, the competing effects of wettability and roughness need to be considered. Kulinich et al. [57] suggested that although superhydrophobic surfaces may exhibit icephobic properties in laboratory conditions, in humid atmospheres, their anti-icing efficiency drops considerably. A humid atmosphere causes water to condense both on top and between the asperities of surfaces, which enhances ice adhesion. In addition, they raised concerns regarding the durability of superhydrophobic surfaces. They observed that after a few icing/deicing cycles, the icephobicity of superhydrophobic surfaces

degrades, and the surface asperities slowly become damaged. Using a model of ice formation on superhydrophobic surfaces, Bahadur et al. [37] proposed that these surfaces would be able to prevent the freezing of impacting droplets up to a temperature of -20 to -25 °C. In spite of these early demonstrations of icephobicity of superhydrophobic surfaces, Nosonovsky and Hejazi [76] asserted that superhydrophobicity is not directly related to icephobicity. It is important to note that the mechanics of ice and water adhesion on a surface differ. Although water is capable of withstanding positive and negative pressures, it is unable to withstand shear stresses. Upon contact with a drop under shear stress, the drop deforms and dewets the surface when the shear force is greater than the counteracting force due to contact angle hysteresis. The situation is different, however, when the drops freeze. Ice is capable of resisting shear and can be detached from a surface by fracture. Shear stress for fracture is determined by the work of adhesion (i.e.  $W_a$ ) and the initial crack dimension. Work of adhesion is a function of receding contact angle. Because of this, superhydrophobic surfaces exhibit low ice adhesion. However, the crack dimension (i.e. the void) at the interface is very important to fracture. It is important to note, however, that even for high values of receding contact angles, the size of the voids at the interface is a critical parameter for icephobicity. Therefore, a comprehensive definition of icephobicity is necessary that accounts for all of these factors.

Icephobicity was defined in terms of four physics: thermodynamics of phase change in supercooled water systems, heat transfer in the formation of ice, mechanics of ice-surface systems, and material characteristics for long-term durability in

mechanical, chemical, and environmental conditions. Each of these factors contributes to the icephobicity of a surface. As a result of this definition, icephobic surfaces possess four main characteristics:

1- The average time needed for ice nucleation of a supercooled droplet on a surface in thermal equilibrium with its surrounding is defined as the average time required for ice nucleation of a supercooled droplet on a surface in thermal equilibrium with its surroundings.

2- The rate of ice accretion on a surface

3 - Adhesion strength at the interface between ice and solid

4 - the icephobicity of a surface over long periods of time.

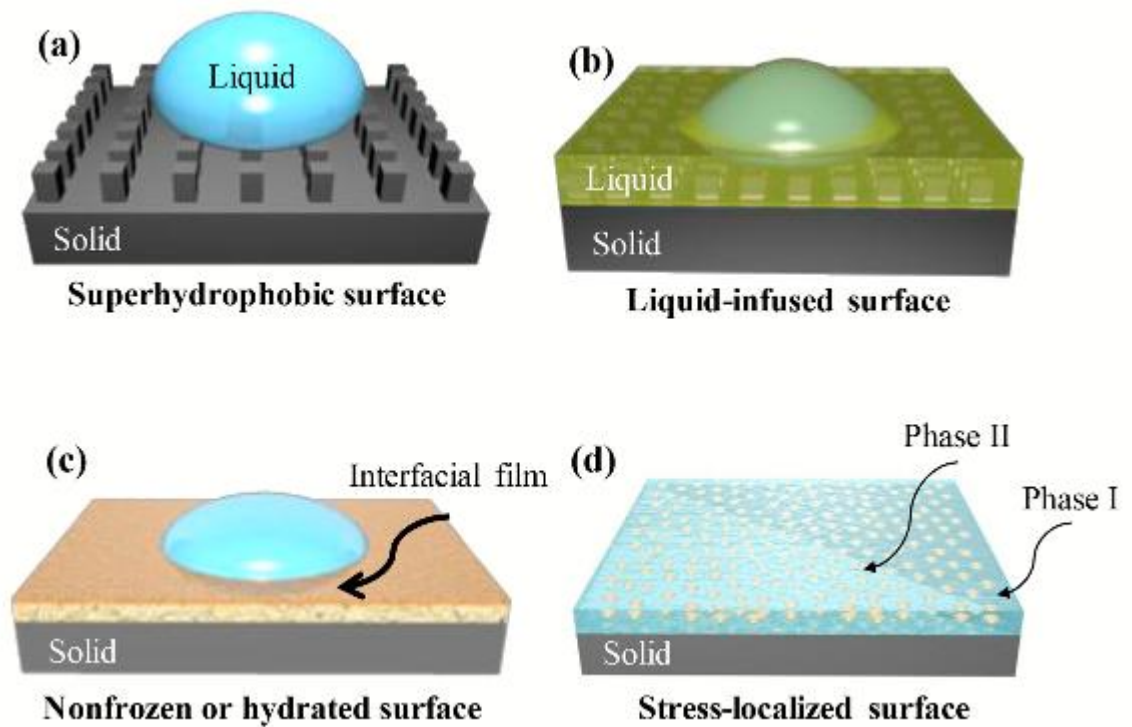


Figure 2 State-of-the-art icephobic surfaces

## Superhydrophobic Surfaces (SHS)

Superhydrophobic surfaces (SHS), Figure 2a, are created through micro/nano structuring on hydrophobic surfaces [115–119] (or hydrophilic surfaces [120,121]). The conditions under which these surfaces trap air and prevent wetting are known as the Cassie-Baxter state and are designed to minimize the effective contact area between stationary or dynamic subcooled droplets and cold solid substrates [18-60]. As a result of their hydrophobic nature, these surfaces affect the thermodynamics of ice nucleation [41,73,75,77,122–125] by controlling parameter in  $f(m,x)$  and the corresponding reduction in solid-ice contact area can influence heat transfer during ice growth (i.e. ice accumulation rate) and the mechanical properties of the solid-ice interface 58,76. As discussed, from a thermodynamic perspective,  $T_N$  is a function of the interfacial energy of solid-water combination and dimension of micro/nano features through Gibbs energy barrier [78,126]. For a given solid, Gibbs energy barrier is not affected unless micro/nano features are dimensionally in the same order as an ice embryo (a few nanometers) [78]. Surfaces with such small features are difficult and expensive to fabricate. Thus, for most studied superhydrophobic surfaces, the median ice nucleation temperature is in the range of  $-20$  till  $-25$  °C [77]. By contrast, the homogeneous ice nucleation temperature of bulk water is  $-40$  °C [127,128], which provides a lower practical limit and target for designing icephobic surfaces where nucleation occurs heterogeneously.  $\tau_{av}$  is also a function of Gibbs energy barrier. At a given temperature, ice nucleation delay time therefore remains unaffected unless the heterogeneous energy barrier is While droplet contact area on superhydrophobic surfaces may be reduced, the

molecular nature of solid-ice interaction (e.g. and the mechanical properties of icephobic surfaces affect ice adhesion strength. The reported ice adhesion on superhydrophobic surfaces is in the order of 100–500 kPa, which is of similar magnitude to adhesion strengths measured on smooth metal surfaces (~100 kPa)[22,59,129–136]. Once frost forms between micro/nano structures on SHS, water droplets sitting on the surface transform into Wenzel state and fill the micro/nano features of the structure. In this case, ice adhesion can become even higher than a smooth surface. Despite extensive studies on the icephobicity of SHS so far, low ice adhesion along with mechanical durability on SHS has not yet been achieved. In a promising approach, Sojoudi et al. [137,138] developed hydrophobic surfaces through grafting of Poly-(1H,1H,2H,2H-perfluorodecylacrylate)(pPFDA) by iCVD method on smooth metals. These surfaces are mechanically durable and reduce ice adhesion on metals by an order of magnitude.

### **Liquid Infused Porous Surfaces (SLIPS)**

Recently, new icephobic surfaces called slippery liquid infused porous surfaces (SLIPS), Figure 2b, have been created, which utilize the smooth nature of liquid surface to improve icephobicity [20,61]. These surfaces were inspired by the *Nepenthes* pitcher plant [139]. SLIPS are developed by entrapping a liquid in a porous media through capillary forces. Despite formation of thin liquid film, the value of  $T_N$  and  $\tau_{av}$  are similar to the superhydrophobic surfaces at  $\sim -25$  °C [140]. The smooth nature of liquid surface mitigates pinning of water droplets on these surfaces [141] and reduce ice adhesion strength [142–155] to values of 10–150 kPa. However, after few cycles of icing-deicing, the liquid layer is depleted and the ice adhesion increases to the order of 200 kPa. This

behavior is discussed in Irajizad et al. [81] and several other studies [153,156–158]. For example, Rykaczewski et al. [65], who studied freezing of sub-cooled condensate on SLIPS, found that water droplets infuse into the bulk of the oil where they form an interface with the solid and deplete oil film as they move on the surface.

### **Liquid Infused Surfaces (LIS)**

In another thoughtful approach, Golovin et al. [165] exploited modified elastomers to reduce ice adhesion. In this approach, the shear modulus of various elastomer was tuned by reducing the cross-linking density of the structure and interfacial slippage was activated at the interface through embedding miscible polymeric chains. The authors reported that the stress required for motion of ice on the surface is in the range of 0.2–10 kPa. However, the stress required for motion of ice on a surface is different than the adhesion stress. While in the former case, ice is still in contact with the surface, in the latter one the induced stress detach ice from the surface. The adhesion stress is the critical stress (maximum stress) that ice detaches from the surface. Furthermore, the adhesion stress on elastomers is a function of shear rate and can vary by an order of magnitude depending on the applied shear rate. Thus, to compare these values of ice adhesion with the other reported values, a standard test protocol needs to be followed. Even recently, Vasileiou et al. [166] showed that flexibility of the substrates could lead to reduce adhesion of ice on a substrate.

## **Interfacial Slippage**

One of the interesting feature of ice is the existence of a thin liquid-like transition layer at the surface even at freezing temperatures, which makes ice slippery [159–163]. This thin film makes it possible to skate at freezing temperatures. This feature has been exploited in development of hydrated icephobic surfaces, Figure 2c, that promote formation of aqueous lubricating layer with no need for additional oil. While the lubricating film exist on the surface (i.e. in the temperature range of 0 to–25 °C), ice adhesion on these surfaces is in the range of 20–60 kPa [27,131,133,164]. However, at lower temperatures, the change in molecular configuration of the transition film drastically boosts the ice adhesion to values in the order of 1000 kPa [27]. The idea of a non-frozen liquid-like layer at the ice surface inspired Chenet al. [62] to develop a new type of icephobic surfaces that keeps a quasi-liquid layer on its surface. These surfaces were developed through blending of polydimethylsiloxane (PDMS)-poly(ethylene glycol) (PEG) amphiphilic copolymers into a polymer matrix and show ice adhesion strength of 50 kPa.

## **Stress-Localized Surfaces (SLS)**

In a recent approach, Irajizad et al. [167] developed concept of stress-localization to reduce adhesion of ice on a surface, Figure 2d. In this approach, a low shear modulus material, phase II, is dispersed in a high shear modulus matrix, phase I. Once ice forms on these surfaces, with a minimal force, ice is detached from phase II

and forms cavities at the interface of ice and the icephobic material. A stress field at the perimeter of cavity is then induced leading to growth of crack/cavity at the interface and fracture. In contrast to other surface-modification approaches (e.g. superhydrophobic, slips and hydrated surfaces), stress-localization effect is a volumetric phenomenon and remains effective even after long-time operation of these surfaces. Ice adhesion on these surfaces is in order of 1–10 kPa while having high mechanical, chemical and environmental durability.

### **Low Interfacial Toughness Surfaces (LITs)**

K. Golovin et al [168] have shown ice accretion has adverse effects on a range of commercial and residential activities. The force required to remove ice from a surface is typically considered to scale with the iced area. This imparts a scalability limit to the use of icephobic coatings for structures with large surface areas, such as power lines or ship hulls. We describe a class of materials that exhibit a low interfacial toughness with ice, resulting in systems for which the forces required to remove large areas of ice (few cm<sup>2</sup> or greater) are both low and independent of the iced area. We further demonstrate that coatings made of such materials allow ice to be shed readily from large areas (~1m<sup>2</sup>) merely by self-weight.

### **Comparison**

We summarized ice adhesion on all reported icephobic surfaces in Figure 3. These include smooth polymers, ceramics and metals to micro/nano structured surfaces and recent advanced surfaces. Variation in the reported ice adhesion for a surface comes

from inconsistency in the measurement's approaches. This graph demonstrates importance of a standard method for ice adhesion assessment. Otherwise, comparison of icephobic performance of different surfaces is not possible.

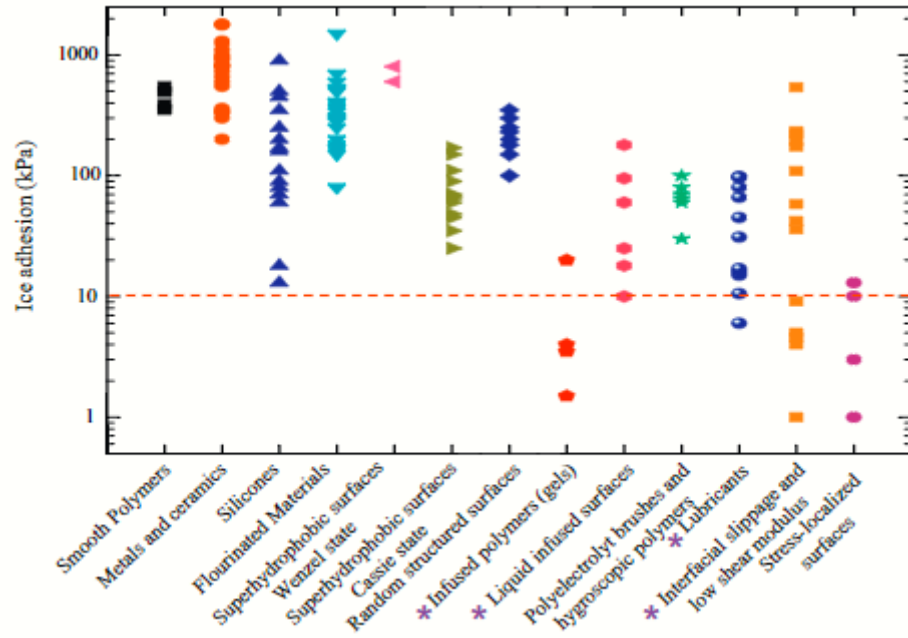


Figure 3 Ice adhesion on state of the art surfaces

Durable icephobic surfaces with ice adhesion smaller than 10 kPa is in high demand in various fields. For most of the surfaces, the measurement method is cuvette-encased ice columns. However, even in this method, the thick-ness of sample and geometrical parameters ( $a$  and  $l$ ) affect measured ice adhesion and a standard protocol needs to be followed. In summary, there is a high demand to explore new material systems along with rational geometrical structuring to develop durable icephobic surfaces. Any proposed icephobic material should be thoroughly examined with all the discussed figures of merit to assure their superior properties. The standard methods elaborated above provide a platform to compare the reports from various laboratories

and guide the scientific community in an optimized approach to find new icephobic materials.

### **III. MERITS FOR INDUSTRIES APPLICATION**

Icephobic surfaces are exposed to various conditions including mechanical abrasion and wear, sand or droplet impact, chemical contaminants, ambient temperature variation, and long-time sun exposure. Thus, to ensure long-time performance, icephobic materials should possess mechanical, chemical and environmental durability. The assessment of these durability for icephobic surfaces should be conducted through standard methods with consistent results across various laboratories. There are two standard methods to assess mechanical durability of icephobic coatings: (I) Taber abrasion test according to ASTM D4060 [104–108] and (II) Hardness test according to ASTM D3363 [109]. In Taber abrasion test, the icephobic sample is placed firmly on a horizontal platform in the Taber instrument and is exposed to an abrader with various loading conditions (e.g. 1, 5, and 10 N). The fine abrader is CS-10, the medium abrader is H-18 and the hard abrader is CS-17. The number of abrasion cycles varies and it can be few cycles to 10,000 cycles.

Durability, which is resistance of a coating against exterior agents that interrupt performance of a coating, is one of the most important characteristics of an icephobic coating to make it practical for commercial applications. There several agents that jeopardize durability of coating which are categorized as environmental, chemical, or mechanical elements. UV-induced oxidation and thermal degradation are environmental elements that weaken durability of a coating. Corrosion and hydrolysis are chemical agents that jeopardize durability of coating. Also, erosion, cracking, abrasion, and detachment of coating from the substrate are categorized as mechanical failures in a

coating. There are several factors that can affect and accelerate each of the mentioned failures. These failures lead to the loss of icephobic properties of a coating. In fact, an icephobic coating is durable that preserves its icephobic properties after many icing/deicing cycles. In this chapter, we are going to introduce elements threaten durability of an icephobic coating and explain the mechanism by which these elements destroy the coating. Also, the factors which affect these mechanisms is explained, since understanding of these factors is important in designing of a durable icephobic coating. At the end of these chapter, standard methods by which durability of a coating is assessed will be explained.

Durability is one of the most important characteristics of icephobic coatings required for practical and long-term applications. Durability is the resistance of coating against exterior stimulus that can change and disrupt performance and characteristics of the coating. The factors affecting durability of a coating can be categorized into environmental, chemical, and mechanical elements. Oxidations by UV radiation and thermal degradation are environmental agents that jeopardize durability of coatings. Hydrolysis through water exposure and corrosion are chemical mechanisms that affect durability of a coating. Erosion, cracking, and abrasion are known as mechanical degradation mechanisms of coatings. In the presence of UV light, photochemical reactions can occur leading to the molecular degradation of the coating. High temperature leads to evaporation of cleavage products and thermal degradation of coating. Also, high temperature as well as swelling by moisture absorption, can lead to volume change that brings about extraction of cleavage products. Hydrolysis in wet

environments causes changes as a result of crosslinking and changes in the structure of coatings. Corrosion resistance is the other property of a durable Icephobic coating. External conditions, such as pH and temperature, in addition to composition of coating have significant effects on the corrosion of a coating. A mechanically durable coating should be resistant to the physical damages, such as scratching and flaking, and mechanical properties of such coating should remain intact during the life-time of the coating. The pressure which is formed on the surface by rain droplets erodes coatings and results in the material loss in the coatings. Abrasive wear of coatings is a common mechanism by which a coating loses its constituents and, as a result, its performance. Due to the internal tensile stress, cracking may occur in a coating leading to the failure of the coating. The degradation processes lead to the changes in the properties of an icephobic coating. Under these changes, the shear modulus of the coating may increase which brings about an increase the ice adhesion to the coating. Under harsh conditions of winter, icephobic coating can be abraded and changes in the thickness of the coating can affect its icephobicity. The color of the coating can be changed which is not desirable in some cases, e.g. in transparent icephobic coatings. Moreover, because of degradation processes, detachment of coating from the substrate can occur. A durable icephobic coating should resist all of these degradation processes. Moreover, icephobic properties of a durable icephobic coating should not change dramatically after many icing/ deicing cycles. <sup>3</sup> Taking all the above mentioned arguments into account, it stands to reason that durability is one of the most important characteristics of an icephobic

coating. Identifying and understanding the degradation mechanisms is critical in the designing of a durable icephobic coating.

### **Ice Adhesion Performance**

Although, ice adhesion on pristine surfaces is the initial metrics to assess performance of icephobic surfaces, the more critical factor is the ice adhesion of these surfaces as they are exposed to various mechanical, chemical, and environmental stimuli which indirectly provide information on long-term performance of these surfaces. For instance, it has been shown that SLIPS surfaces lose their characteristics (i.e. depletion of liquid) after a number of icing and de-icing cycles<sup>43</sup>. We exposed the SLS-PU surfaces to a wide range of harsh environments including 100 icing/deicing cycles, abrasion, water and air jets, long-term UV exposure, high temperature and chemical corrosive environments to assess ice adhesion on these surfaces after these exposures, **Fig. 2b**. As shown, ice adhesion on these surfaces is unchanged due to high durability as we discussed later. Furthermore, as icephobic characteristics of these coatings are volumetric, the abrasion of these surfaces do not change their icephobic characteristics. This is in contrast to surface-functionalized coatings such as superhydrophobic surfaces which lose their characteristics after abrasion.

### **Mechanical Durability**

A comprehensive set of tests were conducted to assess mechanical durability of icephobic surfaces including abrasion, pencil hardness, shore hardness, crosshatch, and most importantly *rain erosion*.

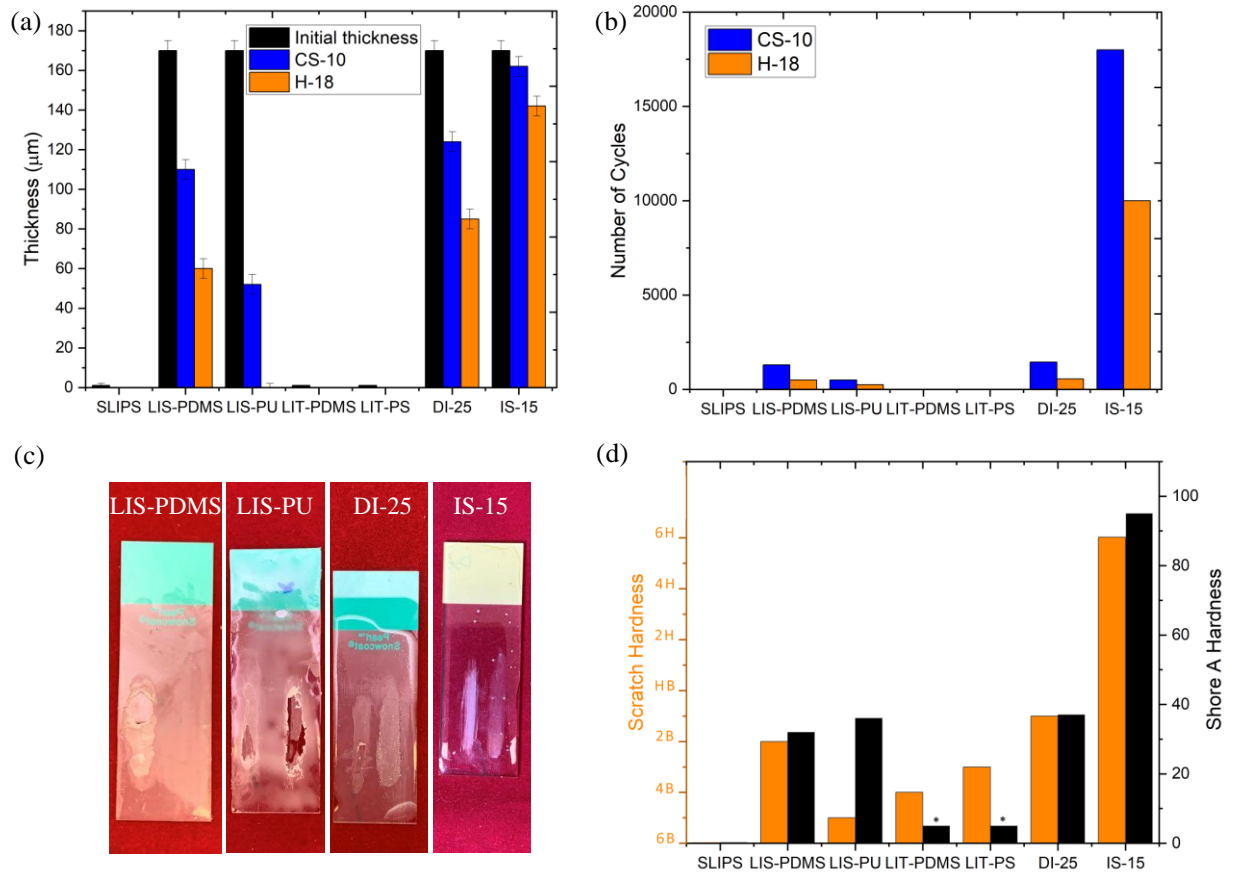


Figure 4 Mechanical durability tests on state-of-the-art icephobic surfaces

In Figure 4 (a) represents the thickness loss by ice shedding surfaces in Taber abrasion metrology is shown. As the thickness of LIT samples are 1-2  $\mu\text{m}$ , they are completely eroded in a few cycles. (b) The number of abrasion cycles is shown in which the coating loses half of its thickness. LIS-PU stands out between all the state-of-the-art ice shedding surfaces. (c) The picture of LIS-PDMS, LIS-PU, LIS-PDMS and LIS-PU after abrasion test are shown. The left trace on each sample denote CS-10 tip and the right one belongs to H-18 tip. (d) Hardness of the ice-shedding surfaces are examined in both Pencil and Shore Hardness metrics. LIS-PU surfaces show scratch hardness of 6H indicating their high scratch resistance.

**Taber Abrasion:** In this metrology, Taber abrasion test (Taber Reciprocating Abrader, Model 5900) were conducted according to ASTM D4060. Samples were placed firmly on a horizontal plate in the Taber instrument and 1000 abrasion cycles were applied. The thickness loss for various samples are shown in Figure 4a. Note that for LIT samples, the low thickness is essential for their icephobic performance. These surfaces are completely abraded after few cycles with soft-tip and the tip touches the underlying glass substrate. To put the abrasion resistance in a better perspective, we measured the number of the cycles to remove half of the thickness of the icephobic coating using both tip of CS-10 and H-10 as shown in Figure 4b. As shown, although LIS-CB provide low ice adhesion, it could not last up more than 400 cycles with tip CS-10 and 100 cycles with the tip H-18. The scenario is somewhat better for DI-25 samples, but still not satisfactory. For the SLS-PU samples, the mechanical durability is far superior to the other surfaces, and it take 100,000 cycles with the hard tip of H-10 to abrade half of the thickness of the coating. The pictures of samples after abrasion test with both tips are shown in Figure 4c to visual comparison of surfaces.

**Pencil Hardness:** This metrology was conducted based on the ASTM D3363. The hardness of the icephobic material is determined by pencil leads of known hardness ranging from 6B to 6H. The scratch resistance of the surfaces is shown in Figure 4d. The SLS-PU shows pencil hardness of 6H.

**Cross Hatch:** This metrology was conducted based on the ASTM D3359. The samples after the crosshatch are classified based on the metric bar of 0-5 as the 0 is the least durable sample and 5 represent the highest durability, Figure 5a. Pictures of the

cross-hatched surfaces are also shown in Figure 5a. SLS-PU had ~0% area removed and is classified at scale 5. This suggests the strong cohesive bonding characteristics of these surfaces.

**Pull-off Adhesion:** The metrology measures adhesion of the icephobic material to the substrate and was conducted according to ASTM D4541. The failure in this experiment could be either adhesive or cohesive. The cohesive failure indicates low durability of the material.

**Water jet:** In this metrology, which is less severe form of rain erosion, the SI surface was placed under a water jet as shown in Figure 5b. The surfaces were kept for 30 mins under water jet and the surface of the samples was visually examined before and after the test. No visual change was detected on the SLS-PU samples. This pre-qualify the surface for the rain erosion metrology.

**Rain Erosion:** The rain erosion is considered as the “the ultimate test” for durability of icephobic materials as these materials will be exposed to external flows. Although surfaces such as SLS-PDMS provide good durability and low ice adhesion, but they fail the rain erosion test. As shown in Figure 5c, the edge of the airfoil is tapped, and the rest of the airfoil is coated with the Spinodal icephobic coating. The tapped portion is removed before the test to have rain droplet hitting the edge of coating-substrate and simulates harsh delamination condition. The water droplets are 1-4 mm in size simulated through 5 water nozzles. The water flow rate is 0.25 m<sup>3</sup>/hr to achieve 7-10 cm of rain fall per hr. The impact speed of the rain droplets is 172 m/s and the test are conducted at ambient temperature. Th test is conducted for three airfoils to have

statistically averaged assessment. The picture of rain eroded SLS-PU is shown in Figure 5c. As shown, the surfaces are intact with no sign of damage or adhesive/cohesive

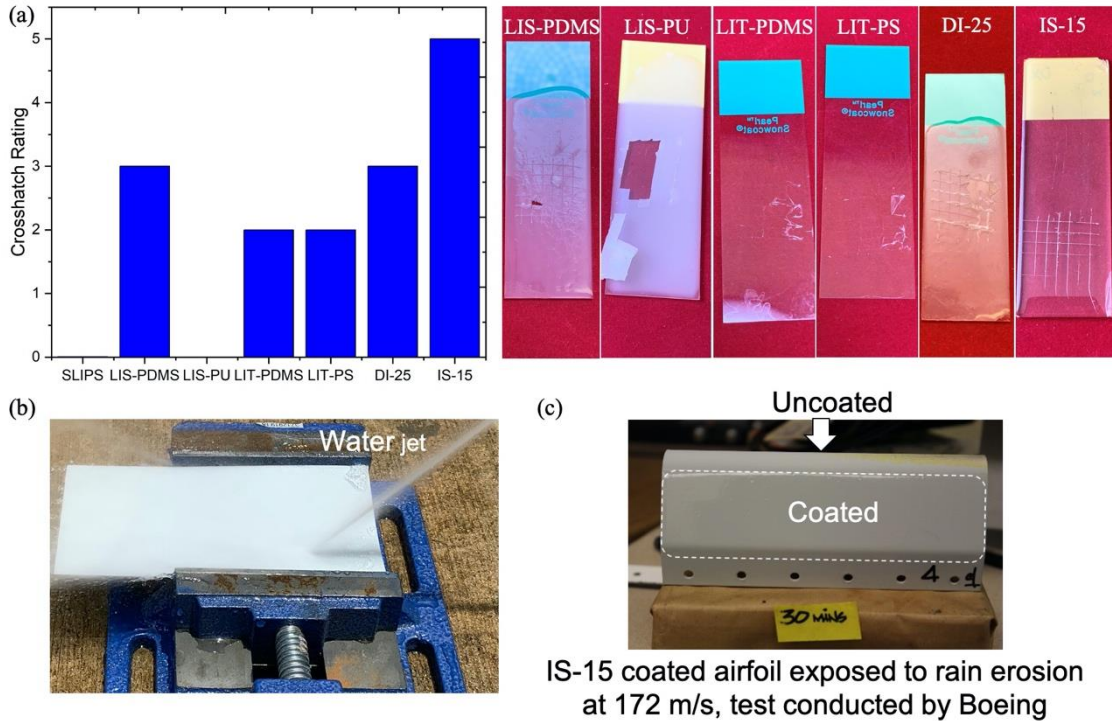


Figure 5 Erosion tests result on state-of-the-art coatings

failure. This ensures the long-term durability of these coatings under freezing rain condition and especially in aerospace applications.

In Figure 5, (a) shows scratch resistance of the ice-shedding surfaces is examined through crosshatch test with cross hatch rating of ~ 5 for SLS-PU (<5% of samples is removed). The picture of cross hatch tests for the ice-shedding surfaces are shown. (b) The SLS-PU surface is shown under water jet test that was kept for 30 mins. (c) The coated airfoil with SLS-PU is shown after the rain erosion test (conducted by Boeing Inc.). Note that the leading edge of the airfoil was kept uncoated to have rain drop impact at the edge of coating-substrate interface. The SLS-PDMS surface was intact with no sign of damage or delamination under the rain erosion speed of 172 m/s.

## **Chemical Resistance**

These tests were conducted in two approaches (1) evaluation of the coating exposed to fluids with various pH at ambient temperature and (2) evaluation of the coating exposed to jet hydraulic fluid and lubricating oils at high temperature,. In the first approach, the coated coupons were immersed in the fluid with pH in the range of 1-11 for 24 hrs. The surface of the samples is examined in terms of softening, blistering and any possible surface damage or change in the integration of the coating. Furthermore, the ice adhesion of these samples was measured as shown above. As shown, the samples are highly durable in the pH range of 3-0, but at lower values of pH, some corrosion to the samples occurs. In the second approach, the samples were immersed in hydraulic oil at temperature of 66 °C and lubrication oil at temperature of 121 °C and were kept for 24 hrs. No possible surface damage or softening should be observed in these tests in order to pass the test.

#### IV. METROLOGY FOR ICE ADHESION

Fundamental understanding of ice formation on a surface, i.e. heterogeneous formation, is critical to suppress ice accretion on the surfaces. Ice formation on a surface includes two steps of ice nucleation and further ice growth. As water droplet is placed on a sub-zero surface, with a time delay, ice nucleolus form on the surface. Ice nucleation is governed by thermodynamics of ice water-surface system and it is described by Gibbs energy barrier,  $\Delta G^*$ , which strongly depends on surface factor,  $f(m, x)$ . Surface factor is a function of surface geometry, i.e. nano or micro, as well as surface free energy and through manipulating these parameters, ice nucleation can be controlled. After ice nucleation, ice further grows in a process which is controlled through heat transfer. Ice growth could be described by two extreme scenarios. In the first one, ice formation occurs with no airflow around where heat transfer through the substrate determines ice growth rate. In the second scenario, ice growth occurs in an environment with external airflow in which ice growth rate is controlled mainly by convective heat transfer. All of mentioned theories about ice formation on a surface are applicable for a single, isolated droplet. However, in reality existence of many droplets on a surface can interfere with ice nucleation and growth of droplets leading to ice bridging phenomenon which is a result of vapor source-sink behavior due to the vapor pressure gradient between a frozen droplet and adjacent liquid droplets

To develop disruptive icephobic surfaces, we must first understand the fundamental phenomena of the solid-ice interface and the effect of length scale on ice formation, ice growth and adhesion. Ice adhesion at the solid-water interface is governed

by phase change thermodynamics at the solid-water interface, heat transfer, and interfacial mechanics.

A comprehensive body of knowledge on these physics allows to cast a set of criteria to assess icephobic surfaces and to rationally develop new icephobic surfaces. We should add that physics of frost nucleation and growth differs from that of ice and is not discussed here. The readers may refer to the cited articles [28,63–71].

### **Ice Nucleation**

As a water droplet touches a subzero surface, it starts to freeze and adhere to the surface. Transformation of a water droplet to ice occurs through a two-step process: (1) Ice nucleation and (2) Ice growth. Ice nucleation temperature,  $T_N$ , is defined as the nucleation temperature of a sessile water droplet which is placed on a sub-zero surface where the total system of water droplet, surface and surrounding environment is cooled down in a quasi-equilibrium condition [1]. One could measure ice nucleation temperature,  $T_N$ , through an isothermal chamber filled with inert gas, e.g.  $N_2$ . The temperature of this chamber is set to  $0^\circ\text{C}$  and a surface is placed in the chamber. At this initial temperature,  $30\ \mu\text{L}$  of distilled water is placed on the surface. Temperature of the substrate is probed with a thermometer to assure isothermal condition. The chamber is cooled down at a rate of  $1\ ^\circ\text{C}/\text{min}$  and ice nucleation of the droplet is monitored with a high-speed camera during the experiment. Ice nucleation temperature is obtained by recording the temperature at which sudden transparency change of the droplet occurs.  $T_N$  is reported as the mean of  $T_N$  measured during a set of more than 10 experiments [1,

2].  $T_N$  is a function of Gibbs energy barrier for heterogeneous ice nucleation which is defined as follows [3]

$$\Delta G^* = \frac{16\pi\gamma_{IW}^3}{3\Delta G_v^2} . \quad (1)$$

In which  $\gamma_{IW}$  is interfacial tension of water-ice nucleolus,  $\Delta G_v$  is the volumetric free energy of phase-change and surface factor,  $f(m,x)$ , is the parameter that affects Gibbs energy barrier for heterogeneous ice nucleation, varies between 0 and 1, and its value is 1 for homogeneous nucleation. An ice nucleolus is a particle which acts as the nucleus for the formation of ice. The initial embryos of ice are formed from a supercooled mother phase, i.e. water droplet, that transform to ice nucleolus when reach to a critical size,  $r_c$ . In this section the focus is mainly on  $f(m,x)$  which is governed by the interfacial free energy and geometry of the interfaces. In  $f(m,x)$ ,  $m$  is a function of interfacial free energies and is defined as

$$m = \cos \theta = \frac{\gamma_{SW} - \gamma_{SI}}{\gamma_{IW}}, \quad (2)$$

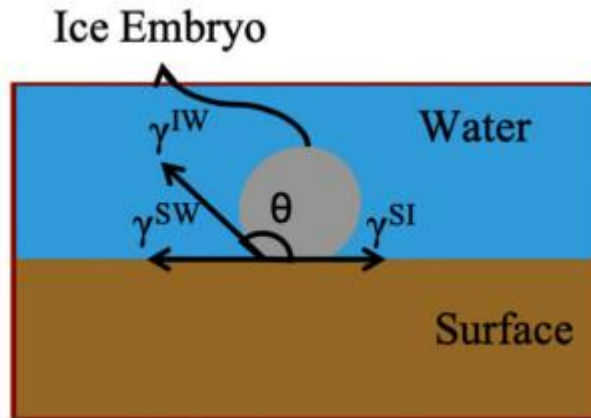


Figure 6. Ice nucleolus on a subzero substrate

where  $\gamma_{sw}$  denotes the solid-water interfacial free energy,  $\gamma_{SI}$  denotes the solid-ice interfacial free energy and  $\gamma_{IW}$  = denotes the water-ice interfacial free energy. These interfaces are illustrated in Figure.

Also,  $x$  which is a function of surface geometry is defined as follows

$$x = \frac{R}{r_c}, \quad (3)$$

where  $R$  is radius of features at the surface and  $r_c$  is the critical nucleolus radius.  $r_c$  is defined in Eq. (4) and its typical value could vary from 1.53 to 4.47 nm for temperature range of -30 to -10°C [3, 4]

$$r_c = \frac{2\gamma_{IW}}{\Delta G_{f,v}}, \quad (4)$$

$$\Delta G_{f,v} = \Delta H_{f,v} \frac{(T_m - T)}{T_m}, \quad (5)$$

$$\text{and } \gamma_{IW} = 23.24 \left( \frac{T}{235.8} \right)^{0.35}. \quad (6)$$

As discussed,  $f(m, x)$  equal to 1 indicates homogeneous nucleation limit and  $f(m, x)$  equal to 0 indicates ice nucleation without sub-cooling. If  $m = 1$  and  $x > 1$ ,  $f$  approaches zero in which case there is no sub-cooling. In order to achieve  $m = 1$ ,  $\gamma_{sw} \geq \gamma_{SI} + \gamma_{WI}$  should be satisfied. If  $m = 1$  and  $x < 1$ , then  $0 < f < 1$ . In this condition, suppression of ice nucleation which is a result of nano-scale confinement occurs.  $f(m, x)$  is analytically derived for two types of surfaces. For convex surfaces,  $f(m, x)$  is defined as

$$f(m, x) = \frac{1}{2} \left\{ 1 + \left( \frac{1 - mx}{g_v} \right)^3 + x^3 \left[ 2 - 3 \left( \frac{x - m}{g_v} \right) + \left( \frac{x - m}{g_v} \right)^3 \right] \right\}, \quad (7)$$

$$\text{where } g_v = (1 + x^2 - 2mx)^{\frac{1}{2}}, \quad (8)$$

and plotted in Figure 7.

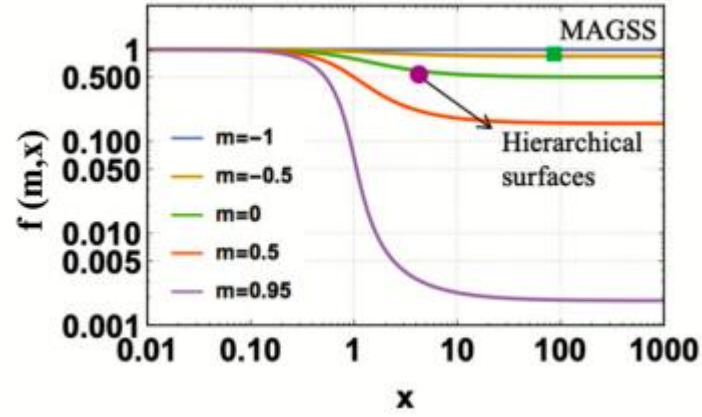


Figure 7 The surface factor for convex surfaces

Also, for concave surfaces  $f(m, x)$  is defined by

$$f(m, x) = \frac{1}{2} \left\{ 1 - \left( \frac{1+mx}{g_c} \right)^3 - x^3 \left[ 2 - 3 \left( \frac{x+m}{g_c} \right) + \left( \frac{x+m}{g_c} \right)^3 \right] + 3mx^2 \left( \frac{x+m}{g_c} - 1 \right) \right\}, \quad (9)$$

$$\text{where } g_c = (1 + x^2 + 2mx)^{\frac{1}{2}} \quad (10)$$

and plotted in Figure 8.

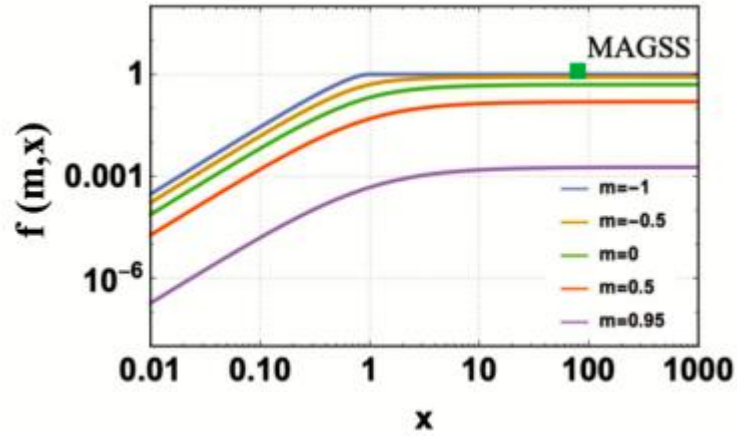


Figure 8 The surface factor plotted for concave surfaces

For  $x$  values larger than 10,  $f(m, x)$  becomes independent of  $x$  and only depends on  $m$  in contrast for  $x$  values less than 10, e.g. when  $R$  is the order of  $r_c$ ,  $f(m, x)$  depends on  $x$  as well [5]. Ice nucleation on a surface depends on the roughness and structure of the surface, i.e. nano or micro surfaces. For example, for  $x < 10$ , ice nucleation on the surface depends on the roughness and structure of the surface, while for  $x > 10$ , surface structure has nothing to do with ice nucleation. In this case, ice nucleation only depends on the interfacial free energies,  $m$ . As an example, nano-grooves on a surface can suppress ice nucleation [6]. Taking all the aforementioned arguments into account, it stands to reason that tuning surface free energy,  $m$  parameter, through different mechanisms is a way to increase ice nucleation energy barrier, especially where the geometry of surface does not affect ice nucleation energy barrier.

On the effect of surface free energy on ice nucleation, according to Eq. (6),  $\gamma_{rw}$  only depends on temperature. Therefore, difference of solid-water surface free energy

and solid-ice surface free energy,  $(\gamma_{sw} - \gamma_{sl})$  is a determining factor in the value of  $\theta$  and as a result in ice nucleation

phenomenon (see Eq. (2)). One of the widely used approaches in the literature is to reduce solid-air interfacial free energy,  $\gamma_{sa}$ . For example, adding functional groups which have high bond dissociation energies, e.g.  $-\text{CF}_3$  and  $-\text{CHF}_2$ , to a surface leads to the reduction of surface free energy. The lowest possible  $\gamma_{sa}$  for a surface is achieved by a monolayer of  $-\text{CF}_3$  groups on a surface and  $\gamma_{sa}$  for such surface is in the range of 6-10 mJ/m<sup>2</sup> [7, 8]. Generally, addition of the materials which contain C-F bonds to a surface reduces its surface free energy,  $\gamma_{sa}$ . For instance, grafting a surface with a monolayer of perfluorodecyltrichlorosilane (FTDS) reduced  $\gamma_{sa}$  and  $\theta$  value of -0.17 is achieved in this case [1]. As another example for implementing this approach, Irajizad and coworkers [2, 9, 10] used the concept of magnetic liquid surfaces and introduced magnetic slippery surfaces (MAGSS) in which a selective ferrofluid is introduced on the surface to tune  $\theta$ ,  $(\gamma_{sw} - \gamma_{sl})$ . On such surface, a liquid-liquid interface is formed by a volumetric magnetic force. These MAGSS show low value of  $m$ , -0.95, which results in the value of 0.98 for  $f(m, x)$ . This condition is pretty close to homogeneous ice nucleation limit, i.e.  $f(m, x) = 1$ . Thus, manipulating  $f(m, x)$  through the modification of surface structure and surface free energy results in an increase in energy barrier of ice nucleation and, as a result, reduction of ice nucleation temperature [5]. The role of  $f(m, x)$  in ice nucleation is illustrated in Figure 9. In the experiment shown in this figure, different surfaces are coated on a cold tube with a temperature of  $-30^\circ\text{C}$ . The tube is exposed to water droplets

and due to high value of  $\Delta G^*$ , i.e. high  $f(m, x)$ , MAGSS showed lowest ice nucleation among other surfaces.

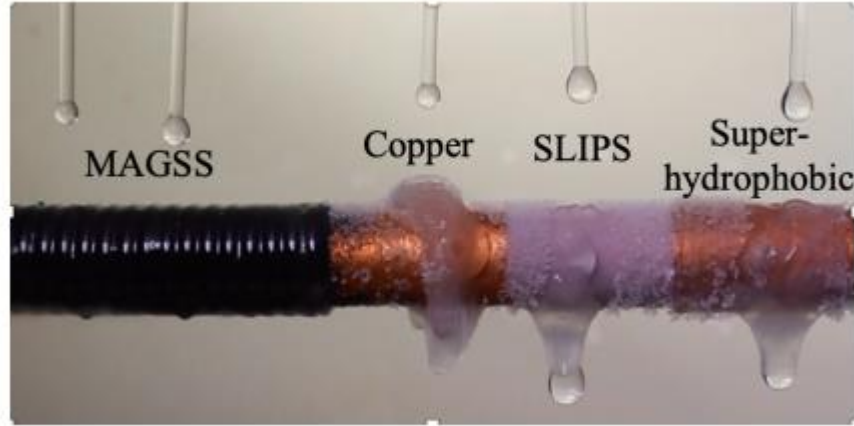


Figure 9 Role of surface factor on ice nucleation on state-of-the-art material

Ice nucleation rate,  $J(T)$ , which is reciprocal of ice nucleation delay time,  $i_4$ , is another metric of ice nucleation.  $i_4$  is defined as the average time required for a supercooled droplet, in equilibrium with its surrounding environment, to nucleate ice phase. In order to measure  $i_4$ , icephobic coating should be initially placed in a cold chamber. Chamber temperature is set to sub-zero temperature and after reaching equilibrium, a water droplet is placed on the coating. At a given temperature, the time required for ice nucleation to occur is recorded and the average time during a set of more than 10 experiments is reported as  $i_4$ . Nucleation rate is defined as follows [3, 11, 12]

$$J(T) = \frac{1}{\tau_{av}} = K \exp\left(-\frac{\Delta G^*}{k_B T}\right), \quad (11)$$

where  $k_B$  is Boltzmann constant and  $K$  is kinetic constant which is defined as [11]

$$K = Z\beta N \quad (12)$$

in which  $N$  denotes number of atomic nucleation sites per unit volume,  $\beta$  denotes the rate of addition of atoms or molecules to the critical nucleus and  $Z$  denotes Zeldovich non-equilibrium factor.

Ice nucleation delay time is an important metric in ice nucleation and depends on  $\Delta G^*$ , as is shown in Eq. (11), which can be tuned by modification of surface roughness and surface free energy. The other approach to increase  $\tau_{av}$  is to increase hydrophobicity of surfaces. In fact, surfaces with higher water contact angle show higher ice nucleation delay times. Basically, by increasing hydrophobicity, value is decreased [13]. Many studies conducted on hydrophobic and superhydrophobic surfaces indicate that  $\tau_{av}$  value for such surfaces, especially for superhydrophobic surfaces, is high. For example, Tourkine et al.[14] grafted fluorinated thiols on a rough copper surface. By doing so, they made a superhydrophobic surface with increased ice nucleation delay time [14]. As another example, Alizadeh et al.[15] developed a superhydrophobic surface by grafting tridecafluoro-1,1,2,2-tetrahydrooctyl-trichlorosilane on a nanostructured silicone surface. By doing so, they boosted ice nucleation delay time [15].

We can rewrite  $J(T)$  in terms of chemical potential,  $\mu$ ,

$$J(T) = K \exp\left(\frac{-8\pi\gamma_{IW}^3}{3 k_B T (\rho\Delta\mu)^2}\right), \quad (13)$$

where  $\rho$  is the molar density of liquid and  $\Delta\mu$  is the chemical potential difference between ice and liquid phase.  $\Delta\mu$  depends on temperature and pressure of the system which can be defined as

$$\Delta\mu(T, P) = \Delta(T, P_{atm}) + (P_L - P_{atm})(v_w - v_i), \quad (14)$$

in an isothermal condition, in which  $v_w$  is specific volume of liquid and  $v_i$  is specific volume of ice.  $P_{atm}$  is atmospheric pressure and  $P_L$  is the liquid pressure which is obtained by Laplace equation

$$P_L - P_{atm} = \frac{2\gamma_{Lv}}{r}, \quad (15)$$

where  $\gamma_{Lv}$  denotes liquid-vapor surface tension and  $r$  is the average radius of curvature. Note that this equation is valid down to few nm scale [16-18]. In fact, the pressure can have either positive or negative effect on ice nucleation. If the  $(v_w - v_i)$  term, which is the slope of solid-liquid phase change line, is positive, pressure increases ice nucleation rate and if the slope is negative, e.g. for water, pressure reduces ice nucleation rate.

The second term on the R.H.S in Eq. (14) is negligible in micro-scale due to high radius of curvature, i.e. the differential between atmospheric and liquid pressure is close to zero (see Eq. (15)). In contrast, the second term is significant in nano-scale, due to the low radius of curvature. For example, the limit of ice nucleation of water, i.e. negative slope of solid-liquid phase change in macro-scale, -38 to -40°C, shifted to lower temperatures at nano-scale. Thus, nano-confined geometry can suppress ice nucleation [19].

## **Ice Growth**

Although ice nucleation is governed by the thermodynamics of ice-water-surface system, further ice growth is controlled by heat transfer. As ice nucleation occurs, release of freezing enthalpy leads to the temperature increase at water-ice interface. In fact, heat transfer at water-ice interface controls ice growth rate. Here, in order to obtain a theory of ice growth, it is assumed that water-ice interface is flat and the curvature at this interface is ignored. Considering this assumption, Gibbs-Thompson undercooling effect becomes negligible. Gibbs-Thomson undercooling effect is the effect of ice-water interface curvature on the temperature of freezing front. This effect

causes the temperature of freezing front to be different from equilibrium melting temperature [20, 21]. We consider that the temperature of freezing front stays at equilibrium temperature of  $T_f$ . In case one considers the undercooling effect ( $\Delta T$ ), the equilibrium temperature at water-ice interface should be replaced by  $T_f - \Delta T$ . Also, airflow around the droplet is a parameter that should be taken into account. To consider airflow effect, two extreme cases of ice growth are defined. The first one is a droplet in an environment without airflow and the second one is a droplet in an environment with airflow surrounding the droplet.

### **Case I: Droplet in an environment without airflow**

In this scenario, tip singularity formation is a common phenomenon that occurs during ice growth. In this phenomenon, when a droplet is placed on a cold plate, it freezes and turns to an ice drop with a pointy tip (Fig. 5). Tip singularity formation is mainly due to the water expansion after freezing and is governed by the quasi-steady heat transfer at the later stages of ice formation. Marín et al. [21] stated that the freezing front is convex at earlier stages of ice growth and at the final stages it becomes concave. They also reported that the freezing front is almost perpendicular to the ice-air interface, i.e.  $\gamma = \phi + \theta \approx 90^\circ$  (see Fig. 5), due to the fact that latent heat cannot transfer across the solid-air interface due to low thermal conductivity of air. The shape of solid-liquid front is obtained through the assumption of constant front temperature at the equilibrium melting temperature,  $T_f$ , i.e. neglecting Gibbs-Thomson effect. For obtaining geometric theory for tip formation, the first step is to write mass conservation with respect to , as temporal dynamics is not significant.

For obtaining geometric theory for tip formation, the first step is to write mass conservation with respect to  $z$ , as temporal dynamics is not significant

$$\frac{d}{dz}(V_l + \nu V_s) = 0, \quad (16)$$

where  $V_l$  and  $V_s$  denote liquid and solid volumes, respectively,  $\nu$  is density ratio, and  $z$  is height of trijunction (Fig. 5). The liquid at the top of freezing front is divided into two parts. The upper part is like a spherical cap with angle of  $\theta$  and the lower part has a volume of  $V_d$ . Thus,

$$V_l = r^3 f(\theta) + V_d, \quad (17)$$

$$\text{and } V_s = -V_d + \int_0^z \pi r(z')^2 dz' \quad (18)$$

Considering the geometries of upper and lower parts of the liquid, one finds,

$$f(\theta) = \frac{\pi}{3} \left( \frac{2-3 \cos \theta + \cos^3 \theta}{\sin^3 \theta} \right), \quad (19)$$

$$\text{and } V_d = r^3 f(\phi) = r^3 f(\gamma - \theta). \quad (20)$$

Based on Eqs. (16–20) and the fact that  $\tan \theta = -\frac{dz}{dr}$ ,  $r(z)$  can be obtained and a sharp tip is formed when  $r \rightarrow 0$ . Thus, at this singularity point, one can find as follows

$$f(\gamma - \theta) + f(\theta) = \nu \left[ f(\gamma - \theta) + \frac{\pi}{3} \tan \theta \right]. \quad (21)$$

Eq. (21) can give volumes of liquid part before and after freezing. If this equation is multiplied by  $r^3$ , the left side gives the volume of liquid. Also, the right side gives the volume of this liquid when it is frozen where expansion factor is considered. According to Eq. (21), we have  $\alpha = \pi - 2\theta$  regardless of  $\nu$  value and as mentioned before  $\gamma \approx$

90°. Therefore, from Eq. (21), a constant value of  $\alpha = 131^\circ$  for the tip angle is obtained which is in a great harmony with the experimental results [21].

Now, we determine the growth rate of ice in scenario one Figure 10. In this case, as the thermal conductivity of air is low, convective heat transfer is low and the generated enthalpy of phase change is transferred through the ice by thermal conduction mechanism and subsequently, through the substrate,  $\vec{q}^s$ . Isothermal condition is assumed for the liquid at the ice-water interface and heat flux through the liquid,  $\vec{q}^l$ , is negligible.

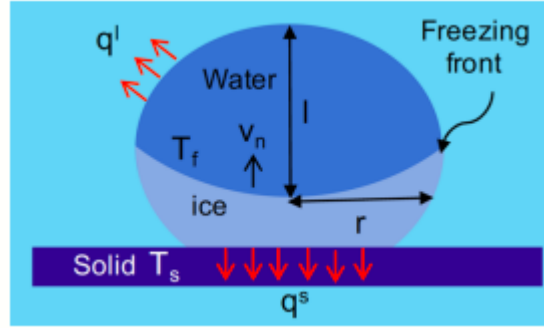


Figure 10 Ice growth on a sub-zero substrate in absence of airflow

$\vec{v}_n$ , the velocity of freezing front is defined as

$$v_n \sim -\frac{dl}{dt} = -\frac{dr(1-\cos\theta)}{\sin\theta}, \quad (22)$$

where  $l$  denotes temporal height and  $r$  denotes the radius of freezing front. The heat transfer away from the interface to the substrate,  $\vec{q}$ , is obtained through the energy balance at the interface for a quasi-steady process as follows

$$\vec{q} = \rho_i \vec{v}_n H_m, \quad (23)$$

where  $\rho_i$  is the density of ice and  $H_m$  is the enthalpy of ice formation. Also, using heat conduction equation,  $\vec{q}$  is obtained as

$$q = -\frac{\delta T}{\left(\frac{l_0-l}{k_i} + \frac{l_m}{k_m}\right)}, \quad (24)$$

where  $\delta T$  denotes the temperature difference between the substrate and ice-water interface ( $T_s - T_f$ ),  $l_0$  denotes initial height of droplet,  $l_m$  denotes the thickness of substrate,  $k_i$  denotes thermal conductivity of ice and  $k_m$  denotes thermal conductivity of substrate. From equations 22, 23 and 24 one finds

$$-\frac{\delta T}{\frac{l_0-l}{k_i} + \frac{l_m}{k_m}} = \rho_i \left(-\frac{dl}{dt}\right) H_m. \quad (25)$$

From Eq. (25) the height ( $l$ ) or radius ( $r$ ) of droplet as a function of time,  $t$ , can be obtained in two different conditions. The first one is for the condition where thermal conductivity of substrate is high or thickness of the coating is low. Thus,  $l_m/k_m \ll l_0/k_i$  and Eq. (25) can be written as

$$l = l_0 - \sqrt{-\frac{2k_i\delta T}{\rho_i H_m}} t. \quad (26)$$

The second condition is when the thermal conductivity of coating is low or the thickness of coating is high. In this case,  $l_m/k_m \gg l_0/k_i$  and Eq. (27) is obtained

$$l = l_0 + \frac{k_m\delta T}{\rho_i H_m l_m} t. \quad (27)$$

The important assumption in the aforementioned analysis is quasi-steady heat transfer. In quasi-steady heat transfer it is assumed that time-scale for ice growth,  $\frac{r}{v_n}$ , is more than thermal diffusion,  $\frac{r^2}{D_i}$  in which  $D_i$  is thermal diffusivity of the ice. This assumption is correct in the case of a water droplet. For example, for a water droplet with 1mm diameter, the time-scale for growth is around 10 s and time-scale for diffusion is around 1 s.

In order to validate the model developed for ice growth rate (Eqs. 26 and 27), Irajizad et al. [5] collected some experimental data on ice growth rate on different substrates. e.g. PDMS<sup>1</sup> and glass. Furthermore, the reported ice growth rate in [22] is included in this comparison. They plotted collected data in Fig. (7) along with ice growth rate obtained from the theoretical model (Eqs. 26 and 27).

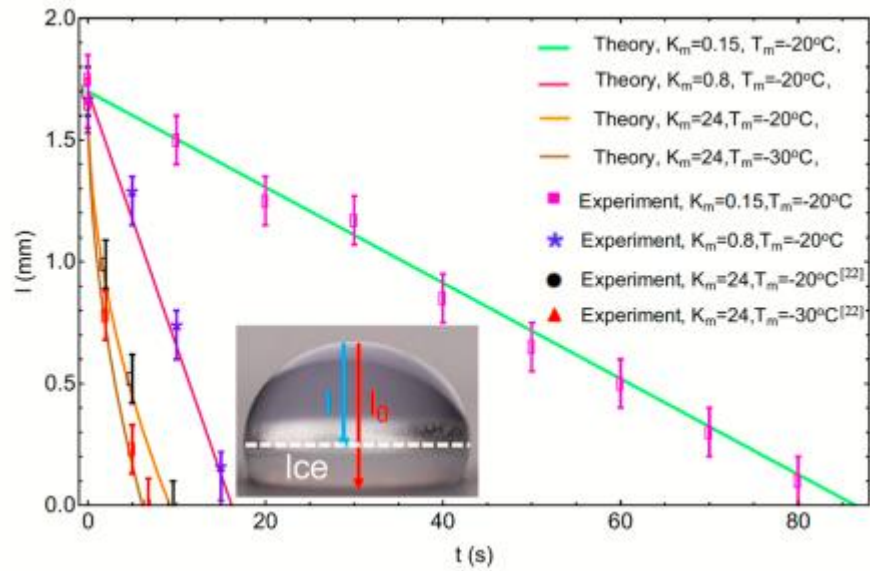


Figure 11 The predicted ice growth rates on a substrate

As shown in Figure 11, the predicted model obtained by heat transfer analysis matches experimental data well [5]. As an example, freezing times of a water droplet on stainless-steel at  $-20^\circ\text{C}$  and  $-30^\circ\text{C}$  are 9.6 and 7 s, respectively, which are obtained from the experiment [23]. The freezing times obtained from predicted model are 10 and 6 s for  $-20^\circ\text{C}$  and  $-30^\circ\text{C}$ , respectively, which are in a great harmony with the experimental data. In order to obtain isotherms in the ice, the heat equation should be solved in the ice domain ( $\nabla^2 T = 0$ ). The boundary conditions in this case are that ice-

water interface temperature is constant and ice-icephobic substrate interface temperature is prescribed.

### Case II: Droplet in an environment with external airflow

Second scenario occurs when there is airflow around the water droplet in which convective heat transfer becomes significant Figure 12. In this case, instead of solid-liquid interface, ice nucleation occurs at liquid-vapor interface, as convective heat transfer reduces temperature at the surface [24]. Fig. (8) shows ice growth pattern for the droplet exposed to an environment with airflow. Similarly to case I, one can use energy balance at phase-changing interface to obtain ice growth rate. The enthalpy released from freezing makes a heat flux at ice-water interface which is carried out with airflow.

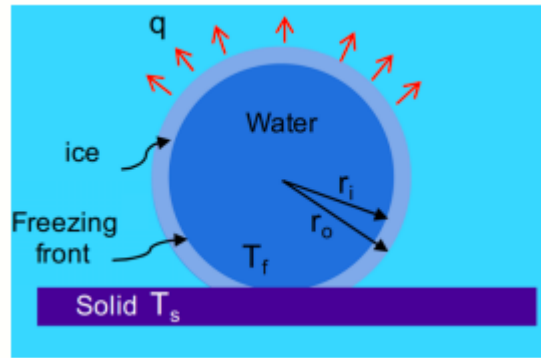


Figure 12 Ice growth on a sub-zero substrate under airflow condition

Similarly to case I, one can use energy balance at phase-changing interface to obtain ice growth rate. The enthalpy released from freezing makes a heat flux at ice-water interface which is carried out with airflow. Thus,

$$\vec{q}_{conv} = \bar{h}_{conv}(T_s - T_\infty), \quad (28)$$

where  $\bar{h}_{conv}$  is convective heat transfer coefficient. In this case, the Nusselt number, written as a function of diameter which is representative dimension ( $Nu_D$ ), by which one can obtain convective heat transfer coefficient, is written as [25]

$$\overline{Nu}_D = \frac{D\overline{h}_{conv}}{k} = 2 + \left(0.4Re_D^{\frac{1}{2}} + 0.06Re_D^{\frac{2}{3}}\right)Pr^{0.4}\left(\frac{\mu}{\mu_s}\right)^{\frac{1}{4}}, \quad (29)$$

where  $Re_D$  is Reynolds number for external airflow,  $Pr$  is Prandtl's number and  $\mu$  is dynamic viscosity. Note that Prandtl's number for air at  $-20^\circ\text{C}$  is 0.75. Considering ice growth, a quasi-steady process, by energy balance at water-ice interface Eq. (23) can be obtained in this case as well. Due to the radial ice growth, the velocity of freezing front is written as

$$\vec{v}_n = \frac{dr_i}{dt}. \quad (30)$$

According to energy balance Eq. (31) could be obtained as

$$\vec{q}A_i = \vec{q}_{conv}A_o, \quad (31)$$

where  $A_i$  is ice-water interface area and  $A_o$  is ice-air interface area. By substituting Eq. (23) and (30) in Eq. (31), the following equation is obtained,

$$\left(\rho_i - \frac{dr_i}{dt}H_m\right)A_i = \bar{h}_{conv}(T_{r=r_0} - T_\infty)A_o. \quad (32)$$

Now, we can find an equation for ice growth rate. Through solution of heat equation in spherical coordinates, we have,

$$\frac{1}{r^2}\frac{\partial}{\partial r}\left(r^2\frac{\partial T}{\partial r}\right) = 0 \rightarrow \frac{\partial T}{\partial r} = \frac{c_1}{r}, \quad (33)$$

$$\text{and, } T = -\frac{c_1}{r} + C_2. \quad (34)$$

$T(r = r_i) = T_f$  and  $T(r = r_o) = T_s$  are ice-water and ice-air interface temperatures, respectively. By applying boundary conditions on Eq. (34), we have,

$$C_1 = -\theta_f \left( \frac{k_i}{hr_0^2} - \frac{1}{r_0} + \frac{1}{r_i} \right)^{-1}, \quad (35)$$

$$\text{and } C_2 = T_\infty + \theta_f \left[ 1 - \left( \frac{k_i r_i}{hr_0^2} - \frac{r_i}{r_0} + 1 \right)^{-1} \right]. \quad (36)$$

$\frac{\theta_s}{\theta_f}$  may be simplified to

$$\frac{\theta_s}{\theta_f} = \frac{k_i r^*}{k_i \left( r^* - \frac{hr_0 r^*}{k_i} + \frac{hr_0}{k_i} \right)}, \quad (37)$$

where Biot number is defined as  $Bi = \frac{hr_0}{k_i}$ .

By writing the energy balance at the ice-water interface one has

$$\vec{q} = hA_o(T_s - T_\infty) = \rho_i H_m A_i \left( -\frac{dr_i}{dt} \right), \quad (38)$$

$$\text{and } h\theta_s = \rho_i H_m \left( -\frac{dr_i}{dt} \right) r^{*2}, \quad (39)$$

and we have the initial condition for ice growth as:  $t(r^* = 1) = 0$ . Thus after few steps of simplification and integration of the energy balance once can finally find

$$t = -\frac{r_0 \rho_i H_m}{6h\theta_f} (2(1 - B_i)r^{*3} + 3B_i r^{*2} - B_i - 2). \quad (40)$$

Through Eq. (40), the radius of ice as a function of time, i.e. ice growth rate, in high air flow condition is obtained. Irajizad et al. [5] plotted Eq. (40) for different air velocities and temperatures. As shown in Fig. (9), the initial rate of ice growth is low. However, the rate of ice growth increases as the ice growth proceeds. Figure 9. The plot of Eq. (40) which shows ice growth rate in an environment with external airflow for different environment temperatures and airflow speeds [5].

A critical factor in ice growth in airflow is humidity. For example, in the presence of airflow, at humidity of 30-75%, ice nucleation occurs at liquid-vapor

interface which is called homogeneous nucleation, while at humidity close to 100%, heterogeneous ice nucleation which is ice nucleation at solid-liquid interface occurs [24]. This phenomenon can be justified by evaporation rate. Evaporation rate is higher at lower humidity. Therefore, at lower humidity high rate of evaporation cools down the liquid-vapor interface leading to ice nucleation at this interface. On the other hand, once evaporation rate is low in high humidity, ice nucleation occurs at solid-liquid interface. Note that humidity also affects ice growth in the environments with airflow. Airflow with higher amount of humidity has higher amount of heat transfer through convection mechanism. In other words, humidity affects convective heat transfer coefficient,  $\bar{h}_{conv}$ .

### **Freezing Delay**

$T_N$  measurement approach: The icephobic sample is placed in a nitrogen chamber with initial temperature of 0 °C. A droplet of distilled water (volume of 30  $\mu$ L) is introduced on the sample's surface at this temperature. The chamber is cooled with cooling rate of 1 °C/10 min. Several thermocouples are installed to probe temperature of the sample and the surrounding environment to ensure isothermal condition. Two thermocouples are attached to the sample with a thermal paste. Temperature of the sample is recorded as close as possible to the droplet without causing disturbance to the experiment. The droplet is visualized with a camera during this cooling process. Once ice nucleates, suddenly the droplet transparency changes and the sample temperature is recorded. This process is repeated for 10 times and the average nucleation temperature is considered  $T_N$  [77,81]. Average nucleation delay time ( $\tau_{av}$ ) is defined as the average time required for ice nucleation of a supercooled droplet in thermal equilibrium with its

surrounding [77].  $\tau_{av}$  measurement approach: The icephobic sample is placed in an isothermal chamber. Temperature of the chamber and the sample are adjusted to a subzero temperature. A water droplet is placed on the sample. The time required for ice nucleation at the given temperature is captured through high-speed imaging of the droplet. Similar to  $T_N$  experiment, one should repeat these experiments for 10 time and report the median time as  $\tau_{av}$ [77,81].

### **Ice Adhesion Strength**

As an icephobic coating is developed, it is crucial to examine icephobic properties including ice adhesion strength to the coating. There are several approaches used in the literature for ice adhesion measurements. Among these approaches, pushing test method, shear test method, centrifugal force method, and tensile force method are widely used. These approaches can be implemented in different setups with various geometries and dimensions. The diversity in ice adhesion measurement methods makes the comparison of reported data difficult and even for the same coating materials different ice adhesion strengths are reported in the literature. Thus, this diversity highlights the importance of introducing a standard approach by which reproducible data can be obtained in different laboratories. In this chapter, we explain the theory of ice adhesion to a surface and derive an equation for the calculation of ice adhesion to the surface of an elastomer. Although this formula is obtained for an elastomer, it can be generalized for the other types of coatings.

## **Methods for measurement**

After that, different approaches which are used for ice adhesion measurement in the literature are discussed. Finally a standard method is proposed which is obtained through the mechanics of ice adhesion to a surface. This standard approach leads to the unification of ice adhesion values obtained from different laboratories with the same metrics.

### **Centrifugal method**

In this method, the icephobic coating is coated at end of a rotating beam as shown in Fig. 3. Ice can be formed on the icephobic coating through placing water inside a mold, e.g. cuvette column, and cooling down it to freeze, or through rain of sub-cooled droplets. The beam starts rotating and induces shear force to the interface between ice and coating. As the rotating speed increases, the induced shear force increases until the ice is detached from the icephobic coating. Ice adhesion strength is defined as the centrifugal force divided by cross-sectional area of detached ice at the moment at which the ice is detached from the icephobic coating. In order to record the moment of detachment, ice separation from the surface is detected by detectors, e.g. piezoelectric cells. The vibrations in the beam during the movement can cause errors in the measurement. These vibrations are mostly due to the imbalance in the beam. In the method introduced by Anti-icing Materials International Laboratory (AMIL), Quebec, Canada, a counter weight can be provided on the other side of beam to decrease such vibrations Figure 13[10].

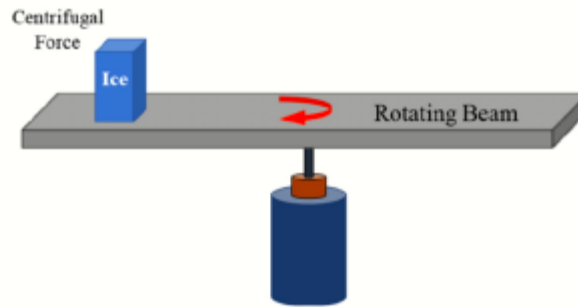


Figure 13 Schematic of centrifugal force method

However, stress at the ice-icephobic substrate interface is complex and shear stress exists mostly on the edges of the samples and dominant stress on the other parts of sample is peel stress. In order to consider this complex, nonuniform stress Adhesion Reduction Factor (ARF) is taken into account. ARF is defined as the adhesion strength of a baseline material, usually aluminum in the centrifugal force method, divided by the adhesion strength of ice to the icephobic coating in the centrifugal force method. This method needs detailed finite element analysis to give quantitative results for the adhesion of ice to the substrate, while without such analysis, it is just a comparison to the baseline material. Sample preparation and ice formation on a substrate are reported in two formats. In the first one, the rotating beam is coated with icephobic coating and the ice is formed on the coating using a mold, e.g. column cuvette, to freeze water[12]. The second way is preparing samples batch off the setup and then fasten the sample on the beam. This method has the benefit of simulating real conditions of ice formation.

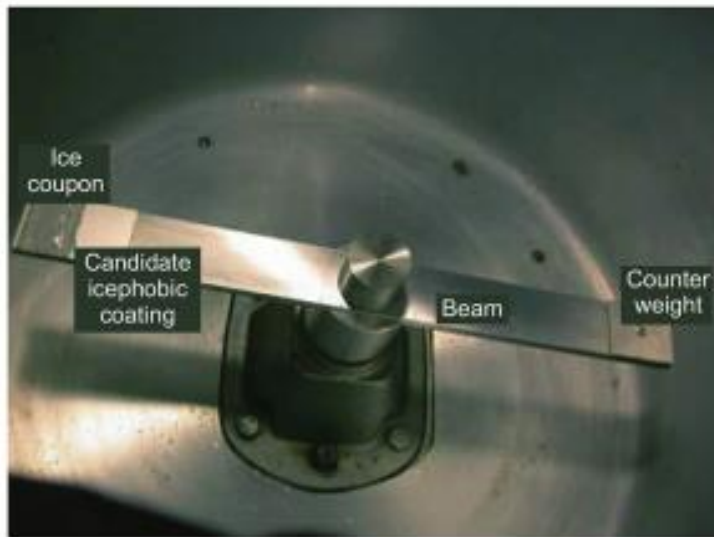


Figure 14 Experimental setup for centrifugal ice adhesion measurement

For example, sample preparation can be conducted in a wind tunnel to make ice as it forms on an airplane. Also, the repeatability of measurements can be assessed in batch off method[10]. However, in these cases, formation of ice in another location and transfer of it to the setup may induce mechanical and thermal stresses on the ice and dissipate frozen stresses, which has significant effects on ice adhesion strength, in the interface. Also, these stresses lead to changes in the ice, e.g. cracking, that alter ice adhesion strength. These stresses are complex and considering them in the ice adhesion measurement is a difficult task. Centrifugal force method has some other drawbacks. The first one is that stress-strain curves for centrifugal force method have not been developed which makes it difficult to analyze results in detail. In addition, it is hard to find the relationship between the strain rate and adhesion strength. Second, the sample is not well-preserved in centrifugal force method making it impossible to go through the sheared interface. Third, ice geometry in centrifugal force method differs near the edges of samples leading to variable stress concentrations. However, this variation is small

and centrifugal force method has shown acceptable reproducibility. The last drawback of centrifugal force method is that vibrations and aerodynamic loadings exist in the experimental setup and may cause error in ice adhesion measurement. However, as mentioned before using a counter weight obviates vibration problems[10]. There is another method in this category called calculated centrifuge adhesion test (CCAT). In this method, the adhesion and tensile strength are calculated according to the distance of pieces of ice from the rotator. While this method obviates in situ issues arising from the centrifugal force method and decreases edge usage, it has some problems. The rotating speed increases as the distance from the center of rotator increases. Thus, ice gathered differs over the length of rotator. In addition, this method does not give accurate information regarding the characteristics of impacted ice[13, 14]. Table 1 summarizes the standard ice adhesion measurement parameters for some icephobic coatings which were obtained by centrifugal force method[6].

Table 1 Ice adhesion measured by centrifugal force method

Surface	Ice Adhesion [kPa]
100/0 PDMS/Silicone Oil	62
85/15 PDMS/Silicone Oil	77
70/30 PDMS/Silicone Oil	41
55/45 PDMS/Silicone Oil	33
50/50 PDMS/Silicone Oil	34
Bare Steel	617
Silicone functionalized steel	127
Nano-micro structured hydrophilic Zn-surface	816
Silicone functionalized-Zn surface	98
Etched Al/ODTMS	90
TiO <sub>2</sub> -Zonyl (Spin coated)	175
TiO <sub>2</sub> -Zonyl (Sprayed)	370

### Peak force method

The second method which is widely used for ice adhesion measurement is the peak force method. In this method, the coated substrate is placed on a cold plate. A mold, e.g. cuvette column, is located on the coating and filled with water to form ice. After ice formation, an increasing force, which can be pushing or pulling, is applied to the test column to detach the ice column from the icephobic coating. The maximum recorded force by a force meter, which is at the moment of ice detachment from the surface, is divided by the ice-substrate interface cross-sectional area to convert it to ice adhesion strength[8]. This method is illustrated in Fig. 1.

The types of mold and applied force in this method are diverse. For example, the mold can be circular or square. However, the square one is preferred to the circular one, since it minimizes possibility of twisting the mold during applying the force[18]. Also, the methods for applying force are diverse. For instance, it can be a needle pushing the ice mold[19-21], a string pulling the mold[18], or a washer on a cylinder and so

on[22-25]. A drawback of the peak force method is that the applied force cannot impact the ice directly. In addition, finite element analysis is needed to be applied on the geometries of tests to correct the obtained data.

Two ways are used to apply force: in the first one, force is applied to the samples individually. In this case, in addition to force transducer, a motion stage can be used to control the velocity of needle or probe[8]. In the second method, the force is applied to all of the samples at the same time and an average of results is reported as adhesion strength. However, this method has a major drawback. As the sample with weakest ice adhesion to the surface is separated, suddenly an increase in the applied force to the other samples occurs which makes them more susceptible to separate from the surface[10, 25]. Also, it is possible to use this method for the impact ice as studied by many researches. Although it is more difficult than non-impact ice. For example, ice can be formed on an airfoil[26] or on a cylinder and disk[27, 28]. Then, the substrate is transferred to the pushing method experimental setup to assess ice adhesion. The ice adhesion measurement can be done by placing, for example, the airfoil into a mold and pushing the ice through the mold[10].

There are some other pushing methods which are used in the literature. For instance, one of these approaches is the two-cylinder method. There are some openings in the outer cylinder through which ice can be formed on the inner cylinder. After ice formation, the outer cylinder rotates and imposes shear force on the ice until ice is removed from the surface. However, in pushing the impacted ice comparison is difficult, since different geometries are implemented[10]. Table 2 summarizes the standard ice

adhesion measurement parameters for some icephobic coatings which were obtained by the peak force method[6].

Table 2 Ice adhesion measured by peak force method

Surface	Ice Adhesion [kPa]
Bare Steel	698
PMMA	463
PC	400
PBMA	384
PDMS (Sylgard 184)	291
PEMA	510
95/5 PEMA/ fluorodecyl POSS	278
70/30 PEMA/ fluorodecyl POSS	166
95/5 Tecnoflon/fluorodecyl POSS	328
70/30 Tecnoflon/fluorodecyl POSS	205
Fluorodecyl POSS	250
pDVB on Si	852
pPFD on Si	284
BL (10nm) on Si	183
BL (40nm) on Si	247
BL (10nm) on Steel	152
BL (40nm) on Steel	199
Pure and Smooth PDMS Film (SF)	750
Porous Film (PF)	2380
Fluorinated Porous Film (FF)	100
AR20 3.1	3.1
AR20+TSF	0.4
PU-0	253
PU-3	92
PU-6	39
PU-9	27
SLIPS	15
Lubricant-Infused Surfaces	10-100
PDMS Mixed with Silicone Oil	1.7
K100-AI	1145
K100-F13-AI	515
F13-Ppy-AI	845
K100-F13-Ppy-AI (SLIPS-AI)	15.6
S-FNM-K103	55
S-NM-K103	55
S-M-K103	55
S-F-K103	55

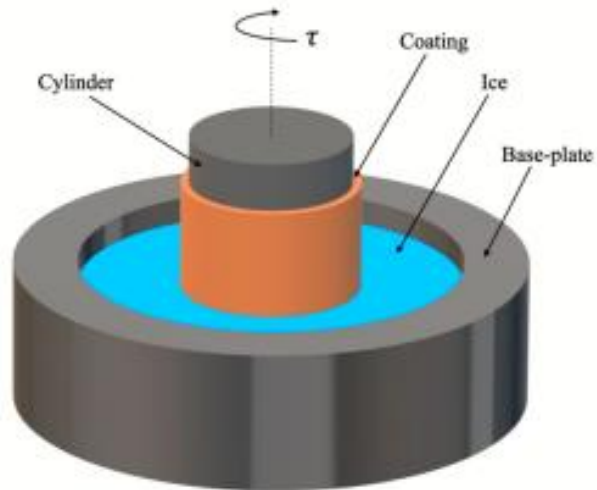


Figure 15 Rotational shear test method

There is another method in this category called the shear test method. Shear tests are categorized, according to the geometry, into rotational shear test[39], lap shear test[40, 41], and  $0^\circ$  cone test[42]. In the rotational shear test a cylindrical or annular setup is used. In the cylindrical form, the cylinder is placed on a massive plate that has walls and forms a lip around the cylinder. Ice is formed in the gap between walls and cylinder. Then, torque is applied through a torsion rod to the cylinder. The cylinder is coated with icephobic coating and ice adhesion on the base-plate is high. Stresses on the edges of cylinder are complex Figure 15. Thus, in order to obviate this problem an annular setup is used in which the base-plate is substituted by another specimen which makes an annular interface that gives higher value of ice adhesion strength[43].

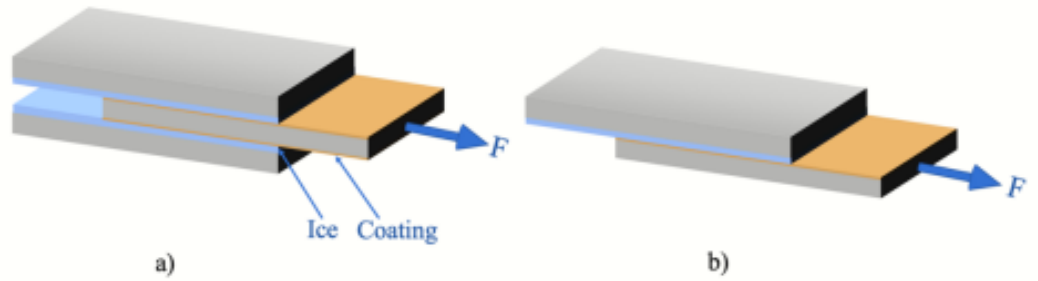


Figure 16 Schematic of shear stress method for ice adhesion measurement

Lap shear test is the second and most widely-used type of shear test that has advantage of low stress concentration[44]. In this method, two flat plates, one of which is coated with icephobic coating, confines ice between themselves. A pushing force is applied to the coated surface to remove ice from the coating. Various formats of lap test are reported in the literature, e.g. single and double-lap shear method. In the double-lap shear method, the icephobic material is coated on both sides of the substrate, and ice is formed in the gaps between coating and substrate according to Figure 16[45].

0° cone test is introduced as a special form of shear test in literature. In this test, instead of two flat plates, an annulus and a cylinder are used. The gap between the rod and hollow cylinder is filled with water to form ice adhering to both surfaces, and the ice adhesion is measured by pushing the inner cylinder out along the common axis with the annulus immobilized[46]. Different loading methods used with similar geometries produce different stress concentrations leading to different ice adhesion measurements. Table 3 summarizes the standard ice adhesion measurement parameters for some icephobic coatings obtained by shear stress methods[6].

Table 3 Ice adhesion measured by peak shear force method

Surface	Ice Adhesion [kPa]
<b>Sylgard 184 (SG 184) 10:1 264</b>	264
<b>SG 184 1:1</b>	14
<b>SG 184 10:1 + 25% 100-cP Silicone Oil</b>	35
<b>SG 184 10:1 + 25% PMHS 10</b>	10
<b>1:9 SG 527:184 + 25% 100-cP Silicone Oil</b>	14
<b>Perfluoropolyether (PFPE) 238</b>	238
<b>PFPE + 25% Krytox 100</b>	31
<b>VytaFlex40 + 20% Vegetable Oil 10.5</b>	10.5
<b>VytaFlex40 + 15% Cod Liver 27</b>	27
<b>VytaFlex40 + 10% 100-cP SO 41</b>	41
<b>VytaFlex40 + 15% Safflower Oil 4</b>	4
<b>VytaFlex40 + 20% Cod Liver 97</b>	97

### **Tensile force method**

The other kind of ice adhesion measurement method is the tensile force method in which tension plays the central role in the ice adhesion measurement, as shown in Figure 17. The setup in this method includes two concentric cylinders between which a gap exists. Cylinder is made of the material which has high ice adhesion, usually aluminum. The outer surface of the inner cylinder is coated with the icephobic coating and the inner surface of the outer cylinder remains intact. The gap between two cylinders is filled with water and is cooled down to freeze. After ice formation in the gap between two cylinders, the setup is located on a tensile machine and a pull force is applied to the inner cylinder which is without coating. Since ice adhesion to the cylinder is high, ice will be removed from the coating on the outer cylinder. At the moment of detachment, the force is recorded and by dividing this force by the area of ice-icephobic coating interface, ice adhesion strength is obtained.

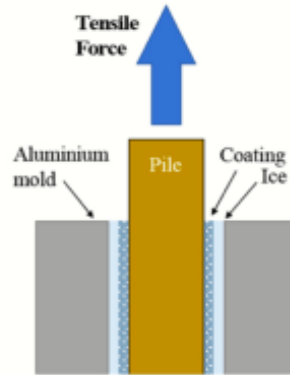


Figure 17 Schematic of tensile force method

In addition to cylindrical geometry, other geometries can be implemented for the tensile force method. For example, ice can be formed in the gap between two square blocks. One of the blocks is coated with icephobic coating and the other block is bare. After ice formation, pull force is applied on the blocks and the ice will be removed from the ice-icephobic coating interface (Figure 18).

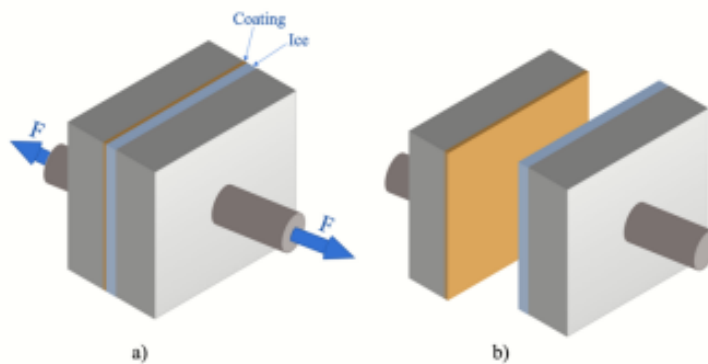


Figure 18 Ice adhesion measurement with the tensile method a) before and b) after detachment

### **Standard Procedure for measurement**

Introducing a standard approach for ice adhesion measurement is important. Lack of such standard method causes the data in the literature not to be comparable to

each other. Also, different ice adhesion values are reported for the same materials in the literature. For example, for PDMS, ice adhesion values are reported in the range of 100-800 kPa[7–9]. Irajizad et al. [6] introduced a standard method for the measurement of ice adhesion that can make the data comparable and uniform. Two important factors should be considered in the developed standard approach which are shear rate and geometry of experimental setup, including  $l$ ,  $a$ , and  $h$  (Figure 19 and Table 4). Regarding the shear rate, in order to detach ice from the surface, shear rate should reach a critical shear rate value at which interface fracture occurs. At shear rates lower than the critical shear rate, ice only slides on the surface and detachment will not occur. Critical shear rate depends on the shear modulus of the material. As the shear modulus increases, critical shear stress decreases [4]. Irajizad et al. [6] stated that for the elastomers with shear modulus in the range of 0.5 MPa-100 MPa and thickness of  $300 \pm 20$  , upper limit for critical shear rate is 0.1 mm/s . The second important factor is the geometry of ice adhesion experimental setup. In the derivation of Eq. (7), some assumptions are considered by which standard parameters can be obtained. The first one is that lubrication approximation of Stoke’s law is used for the determination of hydrostatic pressure field in the elastomer. In order for this approximation to be valid  $a$  and  $h$  should satisfy  $a/h \gg 1$  . Irajizad et al. [6] proposed 15 mm and 300 for the  $a$  and  $h$ , respectively, to satisfy the mentioned condition. The second assumption in the derivation of Eq. (7) is that the vertical displacement of the ice and horizontal length scale have linear relation. For this assumption to be valid,  $l$  and  $a$  should satisfy  $l/a \ll 1$ . Therefore, to satisfy this condition 3 mm for  $l$  value is proposed. Although this standard approach and

mentioned theory in section 2 are obtained based 14 on the assumption that the material is elastomer, it can be generalized to other materials and coatings. Implementing the mentioned standard approach in the ice adhesion measurements leads to reproducible and comparable data obtained in different laboratories.

Ice adhesion measurement method is an important factor in determining the icephobic application of a material. Different methods and approaches used in the literature make the comparison of data impossible. There are several methods used in the literature for ice adhesion measurement among which centrifugal force method, peak force method and tensile force method are three widely-used methods. In all of these methods a force is applied to remove the ice from the icephobic substrate. This force can be in different forms, e.g. centrifugal force which is created by a rotating beam or a tensile force. Different experimental setups with different geometries are used for each of the mentioned methods in the literature which causes the data obtained from the same methods be different from each other. In order to unify ice adhesion measurement results from different laboratories a standard method is proposed. In this standard method, peak force method is selected and shear rate as well as geometry of experimental setup are introduced as two important factors in the designing of experimental setup. In addition, standard values for these two factors are introduced.

Table 4 Parameters for standard ice adhesion measurements

<b>Shear rate</b>	<i>a</i>	<i>h</i>	<i>l</i>
0.1 mm/s	15 mm	300 μm	3 mm

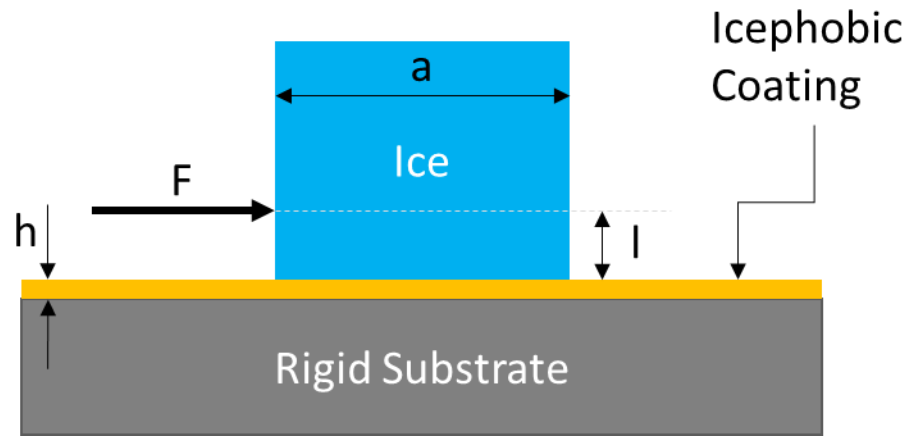


Figure 19 Schematic of standard setup for ice adhesion measurement

## V. CONCLUSION

A comprehensive definition of icephobic surfaces is provided which includes low ice formation temperature, low ice accretion rate, low ice adhesion strength and mechanical, chemical and environmental durability. The ice formation temperature is governed by thermodynamics, ice accretion rate is governed by heat transfer, ice adhesion strength is governed by mechanics of solid-ice interface and durability is governed by the material properties. All these physics are thoroughly discussed and several predictive models are developed and validated by the re-reported data in the literature. Furthermore, the role of length scale in these physics is highlighted. This fundamental physics provides a rational pathway to achieve superior icephobic material. Based on this definition of icephobicity, a set of standard figures of merit is developed for unbiased assessment of icephobic surfaces. Absence of these standard figures of merit has resulted in orders of magnitude discrepancy between reported results for the same icephobic surface by various laboratories. Through the developed comprehensive framework, performance of state-of-the-art icephobic surfaces are compared. The comparison suggests that further research is required to achieve low ice adhesion along with high durability. Furthermore, ice nucleation temperature and ice accretion rate are important metrics which have been overlooked so far. Physics-based and rational approaches are in demand to address these metrics.

## REFERENCES

- [1] Jia, Zongchao, Carl I. DeLuca, Heman Chao, and Peter L. Davies. "Structural basis for the binding of a globular antifreeze protein to ice." *Nature* 384, no. 6606 (1996): 285-288. <https://doi.org/10.1038/384285a0>.
- [2] Liou, Yih-Cherng, Ante Tocilj, Peter L. Davies, and Zongchao Jia. "Mimicry of ice structure by surface hydroxyls and water of a  $\beta$ -helix antifreeze protein." *Nature* 406, no. 6793 (2000): 322-324. <https://doi.org/10.1038/35018604>.
- [3] Dalili, N., Afsaneh Edrisy, and Rupp Carriveau. "A review of surface engineering issues critical to wind turbine performance." *Renewable and Sustainable energy reviews* 13, no. 2 (2009): 428-438. <https://doi.org/10.1016/j.rser.2007.11.009>.
- [4] Andersson, Anna K., and Lee Chapman. "The impact of climate change on winter road maintenance and traffic accidents in West Midlands, UK." *Accident Analysis & Prevention* 43, no. 1 (2011): 284-289. <https://doi.org/10.1016/j.aap.2010.08.025>.
- [5] Gent, Roger W., Nicholas P. Dart, and James T. Cansdale. "Aircraft icing." *Philosophical Transactions of the Royal Society of London. Series A: Mathematical, Physical and Engineering Sciences* 358, no. 1776 (2000): 2873-2911. <https://doi.org/10.1098/rsta.2000.0689>.
- [6] Marwitz, J., M. Poiitovich, B. Bernstein, F. Ralph, P. Neiman, R. Ashenden, and J. Bresch. "Meteorological conditions associated with the ATR72 aircraft accident near Roselawn, Indiana, on 31 October 1994." *Bulletin of the American Meteorological Society* 78, no. 1 (1997): 41-52. <https://doi.org/10.1175/1520-0477>.

[7] Laforte, Jean-Louis, M. A. Allaire, and J. Laflamme. "State-of-the-art on power line de-icing." *Atmospheric Research* 46, no. 1-2 (1998): 143-158. [https://doi.org/10.1016/S0169-8095\(97\)00057-4](https://doi.org/10.1016/S0169-8095(97)00057-4).

[8] Arctic Council. Arctic marine infrastructure; 2009.

[9] Jiang, Xingliang, Jie Zhao, Bing Luo, Jiwu Zhang, and Chunde Huang. "Survey and analysis of ice accidents of early 2008 in southern China." In *The 13th International Workshop on Atmospheric Icing of Structures, Andermatt, Switzerland*, pp. 1-7. 2009.

[10] Antonini, Carlo, Massimiliano Innocenti, Tobias Horn, Marco Marengo, and Alidad Amirfazli. "Understanding the effect of superhydrophobic coatings on energy reduction in anti-icing systems." *Cold Regions Science and Technology* 67, no. 1-2 (2011): 58-67. <https://doi.org/10.1016/j.coldregions.2011.02.006>.

[11] Machielsen, C. H. M., and H. G. Kerschbaumer. "Influence of frost formation and defrosting on the performance of air coolers: standards and dimensionless coefficients for the system designer." *International journal of refrigeration* 12, no. 5 (1989): 283-290. [https://doi.org/10.1016/0140-7007\(89\)90095-9](https://doi.org/10.1016/0140-7007(89)90095-9).

[12] Mohseni, M., and A. Amirfazli. "A novel electro-thermal anti-icing system for fiber-reinforced polymer composite airfoils." *Cold Regions Science and Technology* 87 (2013): 47-58. <https://doi.org/10.1016/j.coldregions.2012.12.003>.

[13] Acharya, Palash V., and Vaibhav Bahadur. "Fundamental interfacial mechanisms underlying electrofreezing." *Advances in colloid and interface science* 251 (2018): 26-43. <https://doi.org/10.1016/j.cis.2017.12.003>.

[14] Homola, Matthew C., Per J. Nicklasson, and Per A. Sundsbø. "Ice sensors for wind turbines." *Cold regions science and technology* 46, no. 2 (2006): 125-131. <https://doi.org/10.1016/j.coldregions.2006.06.005>.

[15] Campbell, Richard J., and Sean Lowry. "Weather-related power outages and electric system resiliency." Washington, DC: Congressional Research Service, Library of Congress, 2012.

[16] LaCommare, Kristina Hamachi, and Joseph H. Eto. "Cost of power interruptions to electricity consumers in the United States (US)." *Energy* 31, no. 12 (2006): 1845-1855.

[17] Research and Markets. [Ice protection systems market - global forecasts to 2021](#); 2017.

[18] Maitra, Tanmoy, Manish K. Tiwari, Carlo Antonini, Philippe Schoch, Stefan Jung, Patric Eberle, and Dimos Poulikakos. "On the nanoengineering of superhydrophobic and impalement resistant surface textures below the freezing temperature." *Nano letters* 14, no. 1 (2014): 172-182. <https://doi.org/10.1021/nl4037092>.

[19] Mishchenko, Lidiya, Benjamin Hatton, Vaibhav Bahadur, J. Ashley Taylor, Tom Krupenkin, and Joanna Aizenberg. "Design of ice-free nanostructured surfaces based on repulsion of impacting water droplets." *ACS nano* 4, no. 12 (2010): 7699-7707. <https://doi.org/10.1021/nn102557p>.

[20] Wong, Tak-Sing, Sung Hoon Kang, Sindy KY Tang, Elizabeth J. Smythe, Benjamin D. Hatton, Alison Grinthal, and Joanna Aizenberg. "Bioinspired self-

repairing slippery surfaces with pressure-stable omniphobicity." *Nature* 477, no. 7365 (2011): 443-447. <https://doi.org/10.1038/nature10447>.

[21] Meuler, Adam J., Gareth H. McKinley, and Robert E. Cohen. "Exploiting topographical texture to impart icephobicity." *ACS nano* 4, no. 12 (2010): 7048-7052. <https://doi.org/10.1021/nn103214q>.

[22] Meuler, Adam J., J. David Smith, Kripa K. Varanasi, Joseph M. Mabry, Gareth H. McKinley, and Robert E. Cohen. "Relationships between water wettability and ice adhesion." *ACS applied materials & interfaces* 2, no. 11 (2010): 3100-3110. <https://doi.org/10.1021/am1006035>.

[23] Alizadeh, Azar, Vaibhav Bahadur, Sheng Zhong, Wen Shang, Ri Li, James Ruud, Masako Yamada, Liehui Ge, Ali Dhinojwala, and Manohar Sohal. "Temperature dependent droplet impact dynamics on flat and textured surfaces." *Applied physics letters* 100, no. 11 (2012): 111601. <https://doi.org/10.1063/1.3692598>.

[24] Alizadeh, A., Yamada, M., Li, R., Shang, W., Otta, S., Zhong, S., Ge, L., Dhinojwala, A., Conway, K.R., Bahadur, V. and Vinciguerra, A.J., 2012. Dynamics of ice nucleation on water repellent surfaces. *Langmuir*, 28(6), pp.3180-3186. <https://doi.org/10.1021/la2045256>.

[25] Guo, Peng, Yongmei Zheng, Mengxi Wen, Cheng Song, Yucai Lin, and Lei Jiang. "Icephobic/anti-icing properties of micro/nanostructured surfaces." *Advanced Materials* 24, no. 19 (2012): 2642-2648. <https://doi.org/10.1002/adma.201104412>.

[26] He, Min, Jianjun Wang, Huiling Li, and Yanlin Song. "Super-hydrophobic surfaces to condensed micro-droplets at temperatures below the freezing point retard

ice/frost formation." *Soft Matter* 7, no. 8 (2011): 3993-4000.  
<https://doi.org/10.1039/c0sm01504k>.

[27] Chen, Jing, Renmei Dou, Dapeng Cui, Qiaolan Zhang, Yifan Zhang, Fujian Xu, Xin Zhou, Jianjun Wang, Yanlin Song, and Lei Jiang. "Robust prototypical anti-icing coatings with a self-lubricating liquid water layer between ice and substrate." *ACS applied materials & interfaces* 5, no. 10 (2013): 4026-4030.  
<https://doi.org/10.1021/am401004t>.

[28] Petit, Julien, and Elmar Bonaccorso. "General frost growth mechanism on solid substrates with different stiffness." *Langmuir* 30, no. 4 (2014): 1160-1168.  
<https://doi.org/10.1021/la404084m>.

[29] Chen, Xuemei, Ruiyuan Ma, Hongbo Zhou, Xiaofeng Zhou, Lufeng Che, Shuhuai Yao, and Zuankai Wang. "Activating the microscale edge effect in a hierarchical surface for frosting suppression and defrosting promotion." *Scientific reports* 3, no. 1 (2013): 1-8. <https://doi.org/10.1038/srep02515>.

[30] Boinovich, Ludmila, Alexandre M. Emelyanenko, Vadim V. Korolev, and Andrei S. Pashinin. "Effect of wettability on sessile drop freezing: when superhydrophobicity stimulates an extreme freezing delay." *Langmuir* 30, no. 6 (2014): 1659-1668. <https://doi.org/10.1021/la403796g>.

[31] Boinovich, Ludmila, and Alexandre M. Emelyanenko. "Role of water vapor desublimation in the adhesion of an iced droplet to a superhydrophobic surface." *Langmuir* 30, no. 42 (2014): 12596-12601. <https://doi.org/10.1021/la503447f>.

[32] Boreyko, Jonathan B., and C. Patrick Collier. "Delayed frost growth on jumping-drop superhydrophobic surfaces." *ACS nano* 7, no. 2 (2013): 1618-1627. <https://doi.org/10.1021/nn3055048>.

[33] Oberli, Linda, Dean Caruso, Colin Hall, Manrico Fabretto, Peter J. Murphy, and Drew Evans. "Condensation and freezing of droplets on superhydrophobic surfaces." *Advances in colloid and interface science* 210 (2014): 47-57. <https://doi.org/10.1016/j.cis.2013.10.018>.

[34] Wang, Shuying, Zhongjia Yang, Guangming Gong, Jingming Wang, Juntao Wu, Shunkun Yang, and Lei Jiang. "Icephobicity of penguins *Spheniscus Humboldti* and an artificial replica of penguin feather with air-infused hierarchical rough structures." *The Journal of Physical Chemistry C* 120, no. 29 (2016): 15923-15929. <https://doi.org/10.1021/acs.jpcc.5b12298>.

[35] Ruan, Min, Wen Li, Baoshan Wang, Binwei Deng, Fumin Ma, and Zhanlong Yu. "Preparation and anti-icing behavior of superhydrophobic surfaces on aluminum alloy substrates." *Langmuir* 29, no. 27 (2013): 8482-8491. <https://doi.org/10.1021/la400979d>.

[36] Wang, Yuanyi, Jian Xue, Qingjun Wang, Qingmin Chen, and Jianfu Ding. "Verification of icephobic/anti-icing properties of a superhydrophobic surface." *ACS applied materials & interfaces* 5, no. 8 (2013): 3370-3381. <https://doi.org/10.1021/am400429q>.

[37] Bahadur, Vaibhav, Lidiya Mishchenko, Benjamin Hatton, J. Ashley Taylor, Joanna Aizenberg, and Tom Krupenkin. "Predictive model for ice formation on

superhydrophobic surfaces." *Langmuir* 27, no. 23 (2011): 14143-14150. <https://doi.org/10.1021/La200816f>.

[38] Sarshar, Mohammad Amin, Christopher Swartz, Scott Hunter, John Simpson, and Chang-Hwan Choi. "Effects of contact angle hysteresis on ice adhesion and growth on superhydrophobic surfaces under dynamic flow conditions." *Colloid and Polymer Science* 291, no. 2 (2013): 427-435. <https://doi.org/10.1007/s00396-012-2753-4>.

[39] Maitra, Tanmoy, Carlo Antonini, Manish K. Tiwari, Adrian Mularczyk, Zulkufli Imeri, Philippe Schoch, and Dimos Poulikakos. "Supercooled water drops impacting superhydrophobic textures." *Langmuir* 30, no. 36 (2014): 10855-10861. <https://doi.org/10.1021/la502675a>.

[40] Hao, Quanyong, Yichuan Pang, Ying Zhao, Jing Zhang, Jie Feng, and Shuhuai Yao. "Mechanism of delayed frost growth on superhydrophobic surfaces with jumping condensates: more than interdrop freezing." *Langmuir* 30, no. 51 (2014): 15416-15422. <https://doi.org/10.1021/la504166x>.

[41] Jung, Stefan, Manish K. Tiwari, N. Vuong Doan, and Dimos Poulikakos. "Mechanism of supercooled droplet freezing on surfaces." *Nature communications* 3, no. 1 (2012): 1-8. <https://doi.org/10.1038/ncomms1630>.

[42] Zhang, Youfa, Xinquan Yu, Hao Wu, and Jie Wu. "Facile fabrication of superhydrophobic nanostructures on aluminum foils with controlled-condensation and delayed-icing effects." *Applied Surface Science* 258, no. 20 (2012): 8253-8257. <https://doi.org/10.1016/j.apsusc.2012.05.032>.

[43] Wen, Mengxi, Lei Wang, Mingqian Zhang, Lei Jiang, and Yongmei Zheng. "Antifogging and icing-delay properties of composite micro-and nanostructured surfaces." *ACS applied materials & interfaces* 6, no. 6 (2014): 3963-3968. <https://doi.org/10.1021/am405232e>.

[44] Boreyko, Jonathan B., Bernadeta R. Srijanto, Trung Dac Nguyen, Carlos Vega, Miguel Fuentes-Cabrera, and C. Patrick Collier. "Dynamic defrosting on nanostructured superhydrophobic surfaces." *Langmuir* 29, no. 30 (2013): 9516-9524. <https://doi.org/10.1021/la401282c>.

[45] Farhadi, Shahram, Masoud Farzaneh, and Sergei A. Kulinich. "Anti-icing performance of superhydrophobic surfaces." *Applied Surface Science* 257, no. 14 (2011): 6264-6269. <https://doi.org/10.1016/j.apsusc.2011.02.057>.

[46] Wang, Nan, Dangsheng Xiong, Yaling Deng, Yan Shi, and Kun Wang. "Mechanically robust superhydrophobic steel surface with anti-icing, UV-durability, and corrosion resistance properties." *ACS applied materials & interfaces* 7, no. 11 (2015): 6260-6272. <https://doi.org/10.1021/acsami.5b00558>.

[47] Ge, Liang, Guifu Ding, Hong Wang, Jinyuan Yao, Ping Cheng, and Yan Wang. "Anti-icing property of superhydrophobic octadecyltrichlorosilane film and its ice adhesion strength." *Journal of Nanomaterials* 2013 (2013). <https://doi.org/10.1155/2013/278936>.

[48] Kulinich, S. A., and M. Farzaneh. "How wetting hysteresis influences ice adhesion strength on superhydrophobic surfaces." *Langmuir* 25, no. 16 (2009): 8854-8856. <https://doi.org/10.1021/la901439c>.

[49] Momen, Gelareh, Reza Jafari, and Masoud Farzaneh. "Ice repellency behaviour of superhydrophobic surfaces: Effects of atmospheric icing conditions and surface roughness." *Applied Surface Science* 349 (2015): 211-218. <https://doi.org/10.1016/j.apsusc.2015.04.180>.

[50] Davis, Alexander, Yong Han Yeong, Adam Steele, Ilker S. Bayer, and Eric Loth. "Superhydrophobic nanocomposite surface topography and ice adhesion." *ACS applied materials & interfaces* 6, no. 12 (2014): 9272-9279. <https://doi.org/10.1021/am501640h>.

[51] Yang, Shuqing, Qiang Xia, Lin Zhu, Jian Xue, Qingjun Wang, and Qingmin Chen. "Research on the icephobic properties of fluoropolymer-based materials." *Applied Surface Science* 257, no. 11 (2011): 4956-4962. <https://doi.org/10.1016/j.apsusc.2011.01.003>.

[52] Tourkine, Piotr, Marie Le Merrer, and David Quéré. "Delayed freezing on water repellent materials." *Langmuir* 25, no. 13 (2009): 7214-7216. <https://doi.org/10.1021/la900929u>.

[53] Mangini, Daniele, Carlo Antonini, Marco Marengo, and Alidad Amirfazli. "Runback ice formation mechanism on hydrophilic and superhydrophobic surfaces." *Cold Regions Science and Technology* 109 (2015): 53-60. <https://doi.org/10.1016/j.coldregions.2014.09.012>.

[54] Mandal, Deepak Kumar, Antonio Criscione, C. Tropea, and A. Amirfazli. "Shedding of water drops from a surface under icing conditions." *Langmuir* 31, no. 34 (2015): 9340-9347. <https://doi.org/10.1021/acs.langmuir.5b02131>.

[55] Graeber, Gustav, Thomas M. Schutzius, Hadi Eghlidi, and Dimos Poulidakos. "Spontaneous self-dislodging of freezing water droplets and the role of wettability." *Proceedings of the National Academy of Sciences* 114, no. 42 (2017): 11040-11045. <https://doi.org/10.1073/pnas.1705952114>.

[56] Varanasi, Kripa K., Tao Deng, J. David Smith, Ming Hsu, and Nitin Bhate. "Frost formation and ice adhesion on superhydrophobic surfaces." *Applied Physics Letters* 97, no. 23 (2010): 234102. <https://doi.org/10.1063/1.3524513>.

[57] Kulinich, S. A., S. Farhadi, K. Nose, and X. W. Du. "Superhydrophobic surfaces: are they really ice-repellent?." *Langmuir* 27, no. 1 (2011): 25-29. <https://doi.org/10.1021/la104277q>.

[58] Sojoudi, Hossein, Minghui Wang, N. D. Boscher, Gareth H. McKinley, and Karen K. Gleason. "Durable and scalable icephobic surfaces: similarities and distinctions from superhydrophobic surfaces." *Soft matter* 12, no. 7 (2016): 1938-1963. <https://doi.org/10.1039/C5SM02295A>.

[59] Hejazi, Vahid, Konstantin Sobolev, and Michael Nosonovsky. "From superhydrophobicity to icephobicity: forces and interaction analysis." *Scientific reports* 3, no. 1 (2013): 1-6. <https://doi.org/10.1038/srep02194>.

[60] Guo, Peng, Yongmei Zheng, Chengcheng Liu, Jie Ju, and Lei Jiang. "Directional shedding-off of water on natural/bio-mimetic taper-ratchet array surfaces." *Soft Matter* 8, no. 6 (2012): 1770-1775. <https://doi.org/10.1039/c1sm06631e>.

[61] Lafuma, A., and D. Quéré. "Slippery pre-suffused surfaces." *EPL (Europhysics Letters)* 96, no. 5 (2011): 56001. <https://doi.org/10.1209/0295-5075/96/56001>.

[62] Chen, Dayong, Martin D. Gelenter, Mei Hong, Robert E. Cohen, and Gareth H. McKinley. "Icephobic surfaces induced by interfacial nonfrozen water." *ACS applied materials & interfaces* 9, no. 4 (2017): 4202-4214. <https://doi.org/10.1021/acsami.6b13773>.

[63] Sun, Xiaoda, Viraj G. Damle, Aastha Uppal, Rubin Linder, Sriram Chandrashekar, Ajay R. Mohan, and Konrad Rykaczewski. "Inhibition of condensation frosting by arrays of hygroscopic antifreeze drops." *Langmuir* 31, no. 51 (2015): 13743-13752. <https://doi.org/10.1021/acs.langmuir.5b03869>.

[64] Nath, Saurabh, and Jonathan B. Boreyko. "On localized vapor pressure gradients governing condensation and frost phenomena." *Langmuir* 32, no. 33 (2016): 8350-8365. <https://doi.org/10.1021/acs.langmuir.6b01488>.

[65] Rykaczewski, Konrad, Sushant Anand, Srinivas Bengaluru Subramanyam, and Kripa K. Varanasi. "Mechanism of frost formation on lubricant-impregnated surfaces." *Langmuir* 29, no. 17 (2013): 5230-5238. <https://doi.org/10.1021/la400801s>.

[66] Walker, Christopher, Sebastian Lerch, Matthias Reininger, Hadi Eghlidi, Athanasios Milionis, Thomas M. Schutzius, and Dimos Poulikakos. "Desublimation frosting on nanoengineered surfaces." *ACS nano* 12, no. 8 (2018): 8288-8296. <https://doi.org/10.1021/acsnano.8b03554>.

[67] Sun, Xiaoda, and Konrad Rykaczewski. "Suppression of frost nucleation achieved using the nanoengineered integral humidity sink effect." *ACS nano* 11, no. 1 (2017): 906-917. <https://doi.org/10.1021/acsnano.6b07505>.

[68] Ahmadi, S. Farzad, Saurabh Nath, Grady J. Iliff, Bernadeta R. Srijanto, C. Patrick Collier, Pengtao Yue, and Jonathan B. Boreyko. "Passive antifrosting surfaces using microscopic ice patterns." *ACS applied materials & interfaces* 10, no. 38 (2018): 32874-32884. <https://doi.org/10.1021/acsami.8b11285>.

[69] Guadarrama-Cetina, Jose, Anne Mongruel, Wenceslao González-Viñas, and Daniel Beysens. "Frost formation with salt." *EPL (Europhysics Letters)* 110, no. 5 (2015): 56002. <https://doi.org/10.1209/0295-5075/110/56002>.

[70] Piucco, Robson O., Christian JL Hermes, Cláudio Melo, and Jader R. Barbosa Jr. "A study of frost nucleation on flat surfaces." *Experimental Thermal and Fluid Science* 32, no. 8 (2008): 1710-1715. <https://doi.org/10.1016/j.expthermflusci.2008.06.004>.

[71] Na, Byeongchul, and Ralph L. Webb. "A fundamental understanding of factors affecting frost nucleation." *International Journal of Heat and Mass Transfer* 46, no. 20 (2003): 3797-3808. [https://doi.org/10.1016/S0017-9310\(03\)00194-7](https://doi.org/10.1016/S0017-9310(03)00194-7).

[72] He, Zhiwei, Senbo Xiao, Huajian Gao, Jianying He, and Zhiliang Zhang. "Multiscale crack initiator promoted super-low ice adhesion surfaces." *Soft Matter* 13, no. 37 (2017): 6562-6568. <https://doi.org/10.1039/c7sm01511a>.

[73] Cao, Liangliang, Andrew K. Jones, Vinod K. Sikka, Jianzhong Wu, and Di Gao. "Anti-icing superhydrophobic coatings." *Langmuir* 25, no. 21 (2009): 12444-12448. <https://doi.org/10.1021/la902882b>.

[74] Zheng, Liqiu, Zhongrui Li, Shawn Bourdo, Khedir R. Khedir, Madhu P. Asar, Charles C. Ryerson, and Alexandru S. Biris. "Exceptional superhydrophobicity and low velocity impact icephobicity of acetone-functionalized carbon nanotube films." *Langmuir* 27, no. 16 (2011): 9936-9943. <https://doi.org/10.1021/la201548k>.

[75] Jung, Stefan, Marko Dorrestijn, Dominik Raps, Arindam Das, Constantine M. Megaridis, and Dimos Poulikakos. "Are superhydrophobic surfaces best for icephobicity?." *Langmuir* 27, no. 6 (2011): 3059-3066. <https://doi.org/10.1021/la104762g>.

[76] Nosonovsky, Michael, and Vahid Hejazi. "Why superhydrophobic surfaces are not always icephobic." *ACS nano* 6, no. 10 (2012): 8488-8491. <https://doi.org/10.1021/nn302138r>.

[77] Eberle, Patric, Manish K. Tiwari, Tanmoy Maitra, and Dimos Poulikakos. "Rational nanostructuring of surfaces for extraordinary icephobicity." *Nanoscale* 6, no. 9 (2014): 4874-4881. <https://doi.org/10.1039/c3nr06644d>.

[78] Fletcher, Neville H. "Size effect in heterogeneous nucleation." *The Journal of chemical physics* 29, no. 3 (1958): 572-576. <https://doi.org/10.1063/1.1744540>.

[79] Li, Chu, Ran Tao, Shuang Luo, Xiang Gao, Kai Zhang, and Zhigang Li. "Enhancing and impeding heterogeneous ice nucleation through nanogrooves." *The*

*Journal of Physical Chemistry C* 122, no. 45 (2018): 25992-25998.  
<https://doi.org/10.1021/acs.jpcc.8b07779> acs.jpcc.8b07779.

[80] Derjaguin, B. V., A. I. Storozhilova, and Ya I. Rabinovich. "Experimental verification of the theory of thermophoresis of aerosol particles." *Journal of Colloid and Interface Science* 21, no. 1 (1966): 35-58.

[81] Irajizad, Peyman, Munib Hasnain, Nazanin Farokhnia, Seyed Mohammad Sajadi, and Hadi Ghasemi. "Magnetic slippery extreme icephobic surfaces." *Nature communications* 7, no. 1 (2016): 1-7.

[82] Irajizad, Peyman, Sahil Ray, Nazanin Farokhnia, Munib Hasnain, Steven Baldelli, and Hadi Ghasemi. "Remote Droplet Manipulation on Self-Healing Thermally Activated Magnetic Slippery Surfaces." *Advanced Materials Interfaces* 4, no. 12 (2017): 1700009. <https://doi.org/10.1002/admi.201700009>.

[83] Masoudi, Ali, Peyman Irajizad, Nazanin Farokhnia, Varun Kashyap, and Hadi Ghasemi. "Antiscalting magnetic slippery surfaces." *ACS applied materials & interfaces* 9, no. 24 (2017): 21025-21033. <https://doi.org/10.1021/acsami.7b05564>.

[84] Russell, Kenneth C. "Nucleation in solids: the induction and steady state effects." *Advances in Colloid and Interface Science* 13, no. 3-4 (1980): 205-318. [https://doi.org/10.1016/0001-8686\(80\)80003-0](https://doi.org/10.1016/0001-8686(80)80003-0).

[85] Mullin, J. W. "Crystallization, Reed Educational and Professional Publishing." (2001).

[86] Liu, Hailong, and Guoxin Cao. "Effectiveness of the Young-Laplace equation at nanoscale." *Scientific reports* 6, no. 1 (2016): 1-10. <https://doi.org/10.1038/srep23936>.

[87] Walther, Jens H., Konstantinos Ritos, Eduardo R. Cruz-Chu, Constantine M. Megaridis, and Petros Koumoutsakos. "Barriers to superfast water transport in carbon nanotube membranes." *Nano letters* 13, no. 5 (2013): 1910-1914. <https://doi.org/10.1021/nl304000k>.

[88] Cottin-Bizonne, Cécile, Catherine Barentin, Élisabeth Charlaix, Lydéric Bocquet, and J-L. Barrat. "Dynamics of simple liquids at heterogeneous surfaces: Molecular-dynamics simulations and hydrodynamic description." *The European Physical Journal E* 15, no. 4 (2004): 427-438. <https://doi.org/10.1140/epje/i2004-10061-9>.

[89] Li, Tianshu, Davide Donadio, and Giulia Galli. "Ice nucleation at the nanoscale probes no man's land of water." *Nature communications* 4, no. 1 (2013): 1-6. <https://doi.org/10.1038/ncomms2918>.

[90] Ajaev, Vladimir S., and Stephen H. Davis. "The effect of tri-junction conditions in droplet solidification." *Journal of crystal growth* 264, no. 1-3 (2004): 452-462. <https://doi.org/10.1016/j.jcrysgro.2003.11.119>.

[91] Marín aG, Enríquez OR, Brunet P, Colinet P, Snoeijer JH. "Universality of tip singularity formation in freezing water drops". *Phys Rev Lett* 2014;113:1-5. <https://doi.org/10.1103/PhysRevLett.113.054301>.

[92] Yao, Yina, Cong Li, Zhenxiang Tao, Rui Yang, and Hui Zhang. "Experimental and numerical study on the impact and freezing process of a water droplet on a cold surface." *Applied Thermal Engineering* 137 (2018): 83-92. <https://doi.org/10.1016/j.applthermaleng.2018.03.057>.

[93] Whitaker, Stephen. "Forced convection heat transfer correlations for flow in pipes, past flat plates, single cylinders, single spheres, and for flow in packed beds and tube bundles." *AIChE Journal* 18, no. 2 (1972): 361-371. <https://doi.org/10.1002/aic.690180219>.

[94] Ryzhkin, Ivan A., and Victor F. Petrenko. "Physical mechanisms responsible for ice adhesion." *The Journal of Physical Chemistry B* 101, no. 32 (1997): 6267-6270. <https://doi.org/10.1021/jp9632145>.

[95] Wilen, L. A., J. S. Wettlaufer, M. Elbaum, and M. Schick. "Dispersion-force effects in interfacial premelting of ice." *Physical Review B* 52, no. 16 (1995): 12426. <https://doi.org/10.1103/PhysRevB.52.12426>.

[96] Chaudhury, M. K., and K. H. Kim. "Shear-induced adhesive failure of a rigid slab in contact with a thin confined film." *The European Physical Journal E* 23, no. 2 (2007): 175-183. <https://doi.org/10.1140/epje/i2007-10171-x>.

[97] Urata, Chihiro, Gary J. Dunderdale, Matt W. England, and Atsushi Hozumi. "Self-lubricating organogels (SLUGs) with exceptional syneresis-induced anti-sticking properties against viscous emulsions and ices." *Journal of Materials Chemistry A* 3, no. 24 (2015): 12626-12630. <https://doi.org/10.1039/C5TA02690C>.

[98] Wang, Chenyu, Trae Fuller, Wei Zhang, and Kenneth J. Wynne. "Thickness dependence of ice removal stress for a polydimethylsiloxane nanocomposite: Sylgard 184." *Langmuir* 30, no. 43 (2014): 12819-12826. <https://doi.org/10.1021/la5030444>.

[99] Susoff, Markus, Konstantin Siegmann, Cornelia Pfaffenroth, and Martina Hirayama. "Evaluation of icephobic coatings—Screening of different coatings and influence of roughness." *Applied Surface Science* 282 (2013): 870-879. <https://doi.org/10.1016/j.apsusc.2013.06.073>.

[100] Kulinich, S. A., and M. Farzaneh. "Ice adhesion on super-hydrophobic surfaces." *Applied Surface Science* 255, no. 18 (2009): 8153-8157. <https://doi.org/10.1016/j.apsusc.2009.05.033>.

[101] Brassard, Jean-Denis, Dilip K. Sarkar, Jean Perron, Annie Audibert-Hayet, and Denis Melot. "Nano-micro structured superhydrophobic zinc coating on steel for prevention of corrosion and ice adhesion." *Journal of colloid and interface science* 447 (2015): 240-247. <https://doi.org/10.1016/j.jcis.2014.11.076>.

[102] Kulinich, S. A., and M. Farzaneh. "On ice-releasing properties of rough hydrophobic coatings." *Cold Regions Science and Technology* 65, no. 1 (2011): 60-64. <https://doi.org/10.1016/j.coldregions.2010.01.001>.

[103] Work, Andrew, and Yongsheng Lian. "A critical review of the measurement of ice adhesion to solid substrates." *Progress in Aerospace Sciences* 98 (2018): 1-26. <https://doi.org/10.1016/j.paerosci.2018.03.001>.

[104] ASTM. Standard test method for abrasion resistance of organic coatings by the taber abraser D4060–10 n.d. ; 2019. <https://doi.org/10.1520/D4060>.

[105] Khanna, Anand S.. High-performance organic coatings. Elsevier, 2008. <https://doi.org/10.1533/9781845694739>.

[106] Rahimi, Hamed, Reza Mozaffarinia, and Akbar Hojjati Najafabadi. "Corrosion and wear resistance characterization of environmentally friendly sol-gel hybrid nanocomposite coating on AA5083." *Journal of Materials Science & Technology* 29, no. 7 (2013): 603-608. <https://doi.org/10.1016/j.jmst.2013.03.013>.

[107] Scrinzi, E., S. Rossi, P. Kamarchik, and F. Deflorian. "Evaluation of durability of nano-silica containing clear coats for automotive applications." *Progress in Organic Coatings* 71, no. 4 (2011): 384-390. <https://doi.org/10.1016/j.porgcoat.2011.04.009>.

[108] Ahmad, Sharif, A. P. Gupta, Eram Sharmin, Manawwer Alam, and S. K. Pandey. "Synthesis, characterization and development of high performance siloxane-modified epoxy paints." *Progress in organic coatings* 54, no. 3 (2005): 248-255. <https://doi.org/10.1016/j.porgcoat.2005.06.013>.

[109] ASTM. Standard test method for film hardness by pencil test D3363–05 n.d. ; 2019. <https://doi.org/10.1520/D3363-05R11E02.2>.

[110] ASTM. Standard test methods for rating adhesion by tape test D3359–17 n.d. ; 2019. <https://doi.org/10.1520/D3359-17>.

[111] ASTM. Standard practice for testing water resistance of coatings in 100% relative humidity n.d. ; 2019. <https://doi.org/10.1520/D2247-15>.

[112] ASTM. Standard test method for evaluation of painted or coated specimens subjected to corrosive environments D1654-08 n.d. ; 2019. <https://doi.org/10.1016/j.snb.2011.06.074>.

[113] ASTM. Standard practice for operating fluorescent Ultraviolet (UV) lamp apparatus for exposure of nonmetallic materials G154-16 n.d. ; 2019. <https://doi.org/10.1520/G0154-16.2>.

[114] Subramanyam, Srinivas Bengaluru, Konrad Rykaczewski, and Kripa K. Varanasi. "Ice adhesion on lubricant-impregnated textured surfaces." *Langmuir* 29, no. 44 (2013): 13414-13418. <https://doi.org/10.1021/la402456c>.

[115] Lafuma, Aurélie, and David Quéré. "Superhydrophobic states." *Nature materials* 2, no. 7 (2003): 457-460. <https://doi.org/10.1038/nmat924>.

[116] Deng, Xu, Lena Mammen, Hans-Jürgen Butt, and Doris Vollmer. "Candle soot as a template for a transparent robust superamphiphobic coating." *Science* 335, no. 6064 (2012): 67-70. <https://doi.org/10.1126/science.1207115> (80-).

[117] Tuteja, Anish, Wonjae Choi, Minglin Ma, Joseph M. Mabry, Sarah A. Mazzella, Gregory C. Rutledge, Gareth H. McKinley, and Robert E. Cohen. "Designing superoleophobic surfaces." *Science* 318, no. 5856 (2007): 1618-1622. <https://doi.org/10.1126/science.1148326> (80- ).

[118] Zhang, Qiaolan, Min He, Jing Chen, Jianjun Wang, Yanlin Song, and Lei Jiang. "Anti-icing surfaces based on enhanced self-propelled jumping of condensed water microdroplets." *Chemical communications* 49, no. 40 (2013): 4516-4518. <https://doi.org/10.1039/c3cc40592c>.

[119] Liu, Jie, Chongqin Zhu, Kai Liu, Ying Jiang, Yanlin Song, Joseph S. Francisco, Xiao Cheng Zeng, and Jianjun Wang. "Distinct ice patterns on solid surfaces with various wettabilities." *Proceedings of the National Academy of Sciences* 114, no. 43 (2017): 11285-11290. <https://doi.org/10.1073/pnas.1712829114>.

[120] Herminghaus, Stephan. "Roughness-induced non-wetting." *EPL (Europhysics Letters)* 52, no. 2 (2000): 165.

[121] Cheng, Yang-Tse, and Daniel E. Rodak. "Is the lotus leaf superhydrophobic?." *Applied physics letters* 86, no. 14 (2005): 144101. <https://doi.org/10.1063/1.1895487>.

[122] Gam-Derouich, Sarra, Jean Pinson, Aazdine Lamouri, Philippe Decorse, Sébastien Bellynck, Remy Herbaut, Laurent Royon, and Claire Mangeney. "Micro-patterned anti-icing coatings with dual hydrophobic/hydrophilic properties." *Journal of Materials Chemistry A* 6, no. 40 (2018): 19353-19357. <https://doi.org/10.1039/C8TA06944A>.

[123] Miljkovic, Nenad, Ryan Enright, and Evelyn N. Wang. "Liquid freezing dynamics on hydrophobic and superhydrophobic surfaces." (2012). <https://doi.org/10.1016/S0040-6090>.

[124] Miljkovic, Nenad, Daniel J. Preston, Evelyn N. Wang, and Ryan Enright. "Ostwald Ripening During Freezing on Scalable Superhydrophobic Surfaces." *Journal of heat transfer* 136, no. 8 (2014): 080901. <https://doi.org/10.1109/ICASSP.2006.1659961>.

[125] Chavan, S., J. Carpenter, M. Nallapaneni, J. Y. Chen, and N. Miljkovic. "Bulk water freezing dynamics on superhydrophobic surfaces." *Applied Physics Letters* 110, no. 4 (2017): 041604. <https://doi.org/10.1063/1.4974296>.

[126] Pruppacher HR, Klett JD. Microphysics of clouds and precipitation. Dordrecht, The Netherlands: Kluwer Academic Publishers; 1997.

[127] Wood, G. R., and A. G. Walton. "Homogeneous nucleation kinetics of ice from water." *Journal of Applied Physics* 41, no. 7 (1970): 3027-3036.

[128] Mossop, S. C. "The freezing of supercooled water." *Proceedings of the Physical Society. Section B* 68, no. 4 (1955): 193. <https://doi.org/10.1088/0370-1301/66/3/311>.

[129] Chen, Jing, Jie Liu, Min He, Kaiyong Li, Dapeng Cui, Qiaolan Zhang, Xiping Zeng, Yifan Zhang, Jianjun Wang, and Yanlin Song. "Superhydrophobic surfaces cannot reduce ice adhesion." *Applied Physics Letters* 101, no. 11 (2012): 111603. <https://doi.org/10.1063/1.4752436>.

[130] Petrenko, Victor F., and S. Peng. "Reduction of ice adhesion to metal by using self-assembling monolayers (SAMs)." *Canadian Journal of Physics* 81, no. 1-2 (2003): 387-393. <https://doi.org/10.1139/p03-014>.

[131] Chen, Jing, Zhiqiang Luo, Qinrui Fan, Jianyong Lv, and Jianjun Wang. "Anti-ice coating inspired by ice skating." *Small* 10, no. 22 (2014): 4693-4699. <https://doi.org/10.1002/sml.201401557>.

[132] Zou, M., S. Beckford, R. Wei, C. Ellis, G. Hatton, and M. A. Miller. "Effects of surface roughness and energy on ice adhesion strength." *Applied surface science* 257, no. 8 (2011): 3786-3792. <https://doi.org/10.1016/j.apsusc.2010.11.149>.

[133] Dou, Renmei, Jing Chen, Yifan Zhang, Xupeng Wang, Dapeng Cui, Yanlin Song, Lei Jiang, and Jianjun Wang. "Anti-icing coating with an aqueous lubricating layer." *ACS applied materials & interfaces* 6, no. 10 (2014): 6998-7003. <https://doi.org/10.1021/am501252u>.

[134] Tarquini, Stefania, Carlo Antonini, Alidad Amirfazli, Marco Marengo, and Jose Palacios. "Investigation of ice shedding properties of superhydrophobic coatings on helicopter blades." *Cold regions science and technology* 100 (2014): 50-58. <https://doi.org/10.1016/j.coldregions.2013.12.009>.

[135] Janjua, Zaid A., Barbara Turnbull, Kwang-Leong Choy, Christos Pandis, Junpeng Liu, Xianghui Hou, and Kwing-So Choi. "Performance and durability tests of smart icephobic coatings to reduce ice adhesion." *Applied Surface Science* 407 (2017): 555-564. <https://doi.org/10.1016/j.apsusc.2017.02.206>.

[136] Bharathidasan, T., S. Vijay Kumar, M. S. Bobji, R. P. S. Chakradhar, and Bharathibai J. Basu. "Effect of wettability and surface roughness on ice-adhesion strength of hydrophilic, hydrophobic and superhydrophobic surfaces." *Applied surface science* 314 (2014): 241-250. <https://doi.org/10.1016/j.apsusc.2014.06.101>.

[137] Sojoudi, Hossein, Hadi Arabnejad, Asif Raiyan, Siamack A. Shirazi, Gareth H. McKinley, and Karen K. Gleason. "Scalable and durable polymeric icephobic

and hydrate-phobic coatings." *Soft Matter* 14, no. 18 (2018): 3443-3454. <https://doi.org/10.1039/c8sm00225h>.

[138] Sojoudi, Hossein, Gareth H. McKinley, and Karen K. Gleason. "Linker-free grafting of fluorinated polymeric cross-linked network bilayers for durable reduction of ice adhesion." *Materials Horizons* 2, no. 1 (2015): 91-99. <https://doi.org/10.1039/C4MH00162A>.

[139] Bohn, Holger F., and Walter Federle. "Insect aquaplaning: Nepenthes pitcher plants capture prey with the peristome, a fully wettable water-lubricated anisotropic surface." *Proceedings of the National Academy of Sciences* 101, no. 39 (2004): 14138-14143. <https://doi.org/10.1073/pnas.0405885101>.

[140] Wilson, Peter W., Weizhe Lu, Haojun Xu, Philseok Kim, Michael J. Kreder, Jack Alvarenga, and Joanna Aizenberg. "Inhibition of ice nucleation by slippery liquid-infused porous surfaces (SLIPS)." *Physical Chemistry Chemical Physics* 15, no. 2 (2013): 581-585. <https://doi.org/10.1039/c2cp43586a>.

[141] Smith, J. David, Rajeev Dhiman, Sushant Anand, Ernesto Reza-Garduno, Robert E. Cohen, Gareth H. McKinley, and Kripa K. Varanasi. "Droplet mobility on lubricant-impregnated surfaces." *Soft Matter* 9, no. 6 (2013): 1772-1780. <https://doi.org/10.1039/c2sm27032c>.

[142] Kreder, Michael J., Jack Alvarenga, Philseok Kim, and Joanna Aizenberg. "Design of anti-icing surfaces: smooth, textured or slippery?." *Nature Reviews Materials* 1, no. 1 (2016): 1-15. <https://doi.org/10.1038/natrevmats.2015.3>.

[143] Kim, Philseok, Tak-Sing Wong, Jack Alvarenga, Michael J. Kreder, Wilmer E. Adorno-Martinez, and Joanna Aizenberg. "Liquid-infused nanostructured surfaces with extreme anti-ice and anti-frost performance." *ACS nano* 6, no. 8 (2012): 6569-6577. <https://doi.org/10.1021/nm302310q>.

[144] Jin, Shenglin, Jie Liu, Jianyong Lv, Shuwang Wu, and Jianjun Wang. "Interfacial materials for anti-icing: beyond superhydrophobic surfaces." *Chemistry—An Asian Journal* 13, no. 11 (2018): 1406-1414. <https://doi.org/10.1002/asia.201800241>.

[145] Stamatopoulos, Christos, Jaroslav Hemrle, Danhong Wang, and Dimos Poulikakos. "Exceptional anti-icing performance of self-impregnating slippery surfaces." *ACS applied materials & interfaces* 9, no. 11 (2017): 10233-10242. <https://doi.org/10.1021/acsami.7b00186>.

[146] Zhang, Guangfa, Qinghua Zhang, Tiantian Cheng, Xiaoli Zhan, and Fengqiu Chen. "Polyols-infused slippery surfaces based on magnetic Fe<sub>3</sub>O<sub>4</sub>-functionalized polymer hybrids for enhanced multifunctional anti-icing and deicing properties." *Langmuir* 34, no. 13 (2018): 4052-4058. <https://doi.org/10.1021/acs.langmuir.8b00286>.

[147] Wang, Nan, Dangsheng Xiong, Yao Lu, Sai Pan, Kun Wang, Yaling Deng, and Yan Shi. "Design and fabrication of the lyophobic slippery surface and its

application in anti-icing." *The Journal of Physical Chemistry C* 120, no. 20 (2016): 11054-11059.

<https://doi.org/10.1021/acs.jpcc.6b04778>.

[148] H a Stone." Ice-phobic surfaces that are wet". *ACS Nano* 2012;6:6536–40. <https://doi.org/10.1021/nn303372q>.

[149] Lv J, Song Y, Jiang L, Wang J. "Bio-inspired strategies for anti-icing". *ACS Nano* 2014;8: 3152–69. <https://doi.org/10.1021/nn406522n>.

[150] Liu Q, Yang Y, Huang M, Zhou Y, Liu Y, Liang X. "Durability of a lubricant-infused electrospray silicon rubber surface as an anti-icing coating". *Appl Surf Sci* 2015; 346:68–76. <https://doi.org/10.1016/j.apsusc.2015.02.051>.

[151] Zhu L, Xue J, Wang Y, Chen Q, Ding J, Wang Q. "Ice-phobic coatings based on silicon oil-infused polydimethylsiloxane". *ACS Appl Mater Interfaces* 2013;5:4053–62. <https://doi.org/10.1021/am400704z>.

[152] Howell, Caitlin, Thy L. Vu, Christopher P. Johnson, Xu Hou, Onye Ahanotu, Jack Alvarenga, Daniel C. Leslie et al. "Stability of surface-immobilized lubricant interfaces under flow." *Chemistry of Materials* 27, no. 5 (2015): 1792-1800. <https://doi.org/10.1021/cm504652g>.

[153] Wexler JS, Jacobi I, Stone HA. "Shear-driven failure of liquid-infused surfaces". *Phys Rev Lett* 2015;114:1–5. <https://doi.org/10.1103/PhysRevLett.114.168301>.

[154] Zhang S, Huang J, Cheng Y, Yang H, Chen Z, Lai Y. “Bioinspired surfaces with super wettability for anti-icing and ice-phobic application: concept, mechanism, and design”. *Small* 2017;13:1–20. <https://doi.org/10.1002/sml.201701867>.

[155] Sun, Jing, Cong Wang, Jinlong Song, Liu Huang, Yankui Sun, Ziai Liu, Changlin Zhao, and Yuxiang Li. "Multi-functional application of oil-infused slippery Al surface: from anti-icing to corrosion resistance." *Journal of Materials Science* 53, no. 23 (2018): 16099-16109. <https://doi.org/10.1007/s10853-018-2760-z>.

[156] Liu Y, Wexler JS, Schönecker C, Stone HA. “Effect of viscosity ratio on the sheardriven failure of liquid-infused surfaces”. *Phys Rev Fluids* 2016;1:1–16. <https://doi.org/10.1103/PhysRevFluids.1.074003>.

[157] Jacobi I, Wexler JS, Stone HA. “Overflow cascades in liquid-infused substrates”. *Phys Fluids* 2015;27. <https://doi.org/10.1063/1.4927538>.

[158] Kim JH, Rothstein JP. “Delayed lubricant depletion on liquid-infused randomly rough surfaces”. *Exp Fluids* 2016;57:1–9. <https://doi.org/10.1007/s00348-016-2171-3>.

[159] Fletcher NH. “Surface structure of water and ice”. *Philos Mag* 1962;7:255–69. <https://doi.org/10.1080/14786436208211860>.

[160] Fletcher NH.” Surface structure of water and ice. II A Revised Model”. *Philos Mag* 1968;18:1287–300. <https://doi.org/10.1080/14786436808227758>.

[161] Ryzhkin I, Petrenko V. “Violation of ice rules near the surface: a theory for the quasiliquid layer”. *Phys Rev B* 2001;65:1–4. <https://doi.org/10.1103/PhysRevB.65.012205>.

- [162] Jellinek HH. “Liquid-like (transition) layer on ice”. *J Colloid Interface Sci* 1967;25: 192–205. [https://doi.org/10.1016/0021-9797\(67\)90022-7](https://doi.org/10.1016/0021-9797(67)90022-7).
- [163] Rosenberg R. “Why is ice slippery?” *Phys Today* 2005; December:50–5. <https://doi.org/10.1063/1.2169444>.
- [164] Wang T, Zheng Y, Raji ARO, Li Y, SikkemaWKA, Tour JM. “Passive anti-icing and active Deicing films”. *ACS Appl Mater Interfaces* 2016;8:14169–73. <https://doi.org/10.1021/acsami.6b03060>.
- [165] Golovin K, Kobaku SPR, Lee DH, DiLoreto ET, Mabry JM, Tuteja A. “Designing durable icephobic surfaces”. *Sci Adv* 2016;2:1–12. <https://doi.org/10.1126/sciadv.1501496>.
- [166] Vasileiou T, Schutzius TM, Poulikakos D. “Imparting Icephobicity with substrate flexibility”. *Langmuir* 2017;33:6708–18. <https://doi.org/10.1021/acs.langmuir.7b01412>.
- [167] Irajizad, Peyman, Abdullah Al-Bayati, Bahareh Eslami, Taha Shafquat, Masoumeh Nazari, Parham Jafari, Varun Kashyap, Ali Masoudi, Daniel Araya, and Hadi Ghasemi. “Stress-localized durable icephobic surfaces”. *Material Horizons* 2019. <https://doi.org/10.1039/C8MH01291A>.
- [168] Golovin, K., Dhyani, A., Thouless, M. D., & Tuteja, A. (2019). “Low–interfacial toughness materials for effective large-scale deicing”. *Science*, 364(6438), 371-375. <https://doi.org/10.1126/science.aav1266>.

[169] Sun X, Damle VG, Liu S, Rykaczewski K. “Bioinspired stimuli-responsive and antifreeze-secreting anti-icing coatings”. *Adv Mater Interfaces* 2015;2:25–7. <https://doi.org/10.1002/admi.201400479>.